Unterschrift Betreuer

DIPLOMARBEIT

Sweep Frequency Response Analysis Applications on Stator Windings of Rotating Machines

ausgeführt am Institut für Angewandte Physik
der Technischen Universität Wien,

in Zusammenarbeit mit *OMICRON electronics* in Klaus,

unter der Anleitung von
Ao.Univ.Prof. Dipl.-Ing. Dr.techn. Martin GRÖSCHL (TU Wien)
Dipl.-Ing. Fabian ÖTTL (OMICRON electronics)
durch

Maximilian MAYER
Matrikelnummer: 01406289

April 2021

Unterschrift Student

Abstract

To avoid the outage of rotating electrical machines, the early detection of deviations from the norm condition is the key element. Particularly noninvasive diagnostic tests are the preferred instrument of choice, especially when they are fast, simple and precise. The sweep frequency response analysis (SFRA), more known in the field of power transformer testing, offers these advantages and is perfectly suited for this task. This thesis focuses on the application potential of SFRA on stators in comparison to the current state-of-the-art diagnostic method, the impulse frequency response analysis (IFRA).

The three analyzed stators have certain properties in common, which allows the detection of characteristics and similarities in certain cases. The stators are manipulated in such a way that inter-turn and inter-winding faults can be implemented and compared. This will also allow for statements about the directionality and sensitivity. Finally, an attempt of a winding extension is made, which reveals the behavior of the two methods applied on longer windings.

A strong focus is placed on practical feasibility, with the research providing results that industrial engineers can apply directly in their work. The research also includes suggestions for an ideal application of the findings in practice.

Kurzfassung

Um Ausfälle rotierender Maschinen zu vermeiden, ist die frühe Diagnose vom Abweichen des Normalzustandes von essentieller Bedeutung. Hierfür sind nichtinvasive diagnostische Tests das bevorzugte Instrument, besonders wenn sie schnell, einfach und hochpräzise sind. Die *Sweep Frequency Response Analysis* (SFRA) bringt diese Eigenschaften mit sich und eignet sich daher hervorragend für diese Aufgabe. Diese Methode wird derzeit hauptsächlich bei Transformatoren angewendet, in dieser Arbeit wird jedoch ihre Tauglichkeit für die Untersuchung von Statoren geprüft. Um die Ergebnisse zu quantifizieren, werden sie mit der *Impulse Frequency Response Analysis* (IFRA), einem derzeit verbreiteten Diagnoseverfahren für Statoren, verglichen.

Die drei analysierten Statoren haben einzelne Eigenschaften gemein, welche Rückschlüsse auf Charakteristika und Ähnlichkeiten der Ergebnisse ermöglichen. Die Statoren wurden so manipuliert, dass Windungs- und Wicklungsschlüsse implementiert werden können. Des Weiteren werden Aussagen über die Sensitivität und die Richtungsabhängigkeit getroffen. Zuletzt wurde eine Wicklungsverlängerung simuliert, um Angaben über das Verhalten der beiden Methoden bei ausgedehnteren Leitungen zu machen.

Einen starken Fokus wurde auch auf die praktische Umsetzbarkeit der Methode gelegt um Ergebnisse zu erzielen, die direkt vom Endanwender übernommen werden können. Hierzu werden auch Empfehlungen abgegeben, wie die gewonnenen Erkenntnisse am besten in der Praxis umsetzbar sind.

List of Abbreviations

DUT	Device Under Test
IFRA	Impulse Frequency Response Analysis
IWT	Impulse Winding Tester
PE	Protective Earth
PTM	*Primary Test Manager*
P1	Phase 1
P2	Phase 2
P3	Phase 3
R_{LF}	Relative Factor of the Low Frequency Range
SFRA	Sweep Frequency Response Analysis
ZC	Zero Crossing

Table 0.1: List of Abbreviations

Contents

1 Introduction

1.1 Motivation

A reliable operation of generators and motors is essential for a continuous energy and industrial production. Any outage of such devices can lead to immense costs. At the root of such failures are often various smaller malfunctions, which be prevented by prescient maintenance with highly sensitive diagnostic equipment. [8] [2] Furthermore, the number of electric vehicles is rising rapidly, and nearly all of them are running three-phase induction motors, which have to be investigated during maintenance or after incidents.

Currently, a common diagnostic method for rotating machines is the impulse frequency response analysis (IFRA or surge test). However, as has repeatedly been reported, the sensitivity of the method was not high enough to detect all the potential issues. Therefore, the search for an alternative method was initiated. One potential replacement could be the sweep frequency response analysis (SFRA). The goal of this theses is to evaluate the sensitivity of this method and to investigate the practicability of the approach.

Primarily, SFRA is a standardized, low-voltage, noninvasive diagnostic test for power transformers. [15] Its sensitivity and other advantages equip it perfectly for further tasks and applications, for example for testing the condition of rotating machines. [7] The SFRA is able to detect various deviations from the electrical and mechanical normality caused by deformations, insulation fatigue, or short faults.

1.2 Overview

The theory presented in chapter 2 explains the two compared frequency response analyses, SFRA (2.1) and IFRA (2.2). The corresponding quantifying methods for each FRA are elaborated in the particular subsections 2.1.1 and 2.2.1.

Chapter 3 introduces the setup of the experiment. First, the properties of the three stators are explained, with a specific focus on the winding structure (3.1.1). Second, the preparation and installation of the access points (3.1.2) are carried out before, third, the

used equipment (3.2) is listed and explained.

The results are discussed in chapter 4 and are split up into different fault cases. For every fault case, the same scheme is used: first, the SFRA measurement is clarified and discussed, then the findings are compared to the results of the same setup measured with the IFRA method. Afterwards, the differences and advantages of each technique are reconsidered and evaluated.

A special focus is put on inter-turn and inter-winding faults (4.2 and 4.3). A single inter-turn fault describes a short circuit within one winding, which bypasses only one single turn of the winding. If two turns of parallel circuits (can be within the same phase) are short circuited, it is called an inter-winding fault.

Chapter 5 reviews the results and the gained operating experience. In addition, an outlook is provided for future applications of SFRA, combined with examples for their use.

2 Theory

The term *frequency response* is defined by the Institute of Electrical and Electronics Engineers as "the frequency dependent relation in both gain and phase difference between steady-state sinusoidal inputs and the results steady-state sinusoidal outputs" in stable, linear systems. [5]

The DUT (Device Under Test) can be seen as a composition of many distributed, unknown RLC parts, respectively a *black box*. This black box has a characteristic, complex, and frequency dependent transfer function $H(f)$, which is applied on the signal passing through the device (figure 2.1 left). [5] [9]

Simplified, the RLC network of the DUT depends on the capacitance between the single turns of the windings, the capacitance between winding and environment (chassis, core, etc.), the induction of the winding, and the resistance of the leads (figure 2.1 right). [14]

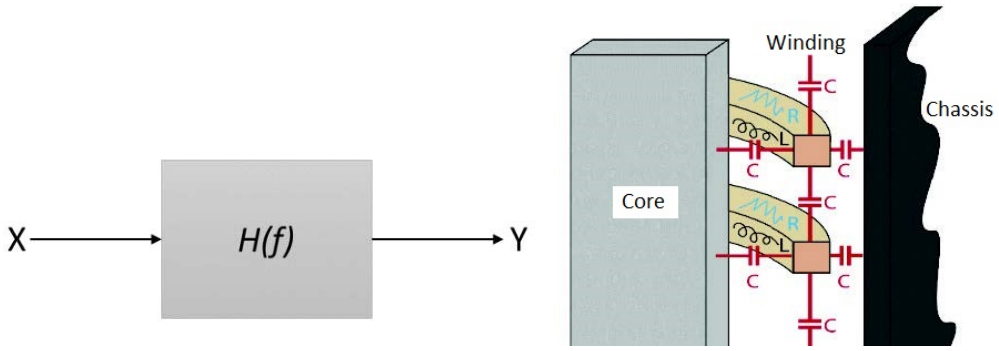

Figure 2.1: Left: input signal X and output signal Y emerging the black box with its transfer function $H(f)$; Right: RLC network of a power transformer. [21]

Frequency response analysis (FRA) procedures are based on the comparison of at least two measurements. [6] The outcome of the current test is compared to either an older measurement of the same phase of the same device (fingerprint), another phase of the same device, or sister units of the device (identical in design). [18] In the future, there could be computer generated curves, based on the DUTs properties.

The fingerprint comparison contains the most information about small variations inside

the DUT, but they are not always available, especially for new (not yet standardized) tests like SFRA. The comparison to other phases usually differs a little bit since the leads can vary slightly in length and design. In principle, sister units have identical properties, according to their data sheet, but since coils in induction motors are mostly random wound, they can have different characteristics. Therefore, the measurements can diverge, even if both windings are in a proper condition, and a comparison is only under certain circumstances acceptable.

2.1 Sweep Frequency Response Analysis

For a SFRA measurement a low-voltage, sinusoidal signal with variable frequency is applied to the DUT. At the input terminal the amplitude and phase of the signal are used as the reference signal $U_{input}(f)$, at the output terminal the response signal is measured as $U_{output}(f)$. [4]

The transfer function $H(f)$ depends on the impedance Z of the DUT and the measuring equipment and, therefore, on the frequency of the injected signal (equation 2.1). The frequency response of the amplitude k is the ratio of the output voltage to the reference signal (equation 2.2). The resulting function depends on the frequency f and is given in decibel. The calculation of the phase angle between the signals is shown in equation 2.3 and is also frequency-dependent. [15]

$$H(f) = \frac{U_{output}(f)}{U_{input}(f)} = \frac{Z_{SFRAequipment}}{Z_{SFRAequipment} + Z_{DUT}} \tag{2.1}$$

$$k = 20 \cdot log \left[\frac{U_{output}}{U_{input}} \right] \tag{2.2}$$

$$\varphi = \arctan \left[\frac{\angle U_{output}}{\angle U_{input}} \right] \tag{2.3}$$

For an accurate result, it is necessary to use identical leads for the response and reference channels, otherwise the impedance $Z_{SFRAequipment}$ of the reference would differ from $Z_{SFRAequipment}$ of the response. [4]

The frequency range of a SFRA test usually starts at 20 Hz and rises up to 2 MHz, applied voltages are typically between 0.1 V and 10 V. [15]

2.1.1 Relative Factor

There are several methods for quantifying the measurement results gained with SFRA, i. e. procedures how two amplitude and phase plots can be compared. One of them is the calculation of the relative factor: Since the outcome of a SFRA measurement contains discrete values, the cross correlation or, more commonly, the relative factor (an alternation of the cross correlation) can be calculated. The relative factor R_{xy} describes the similarity of two curves or sequences of functions with real values ($X(k)$ and $Y(k)$) and length $k = 0, 1, \ldots, N-1$. For the following calculation of R_{xy}, the variables under the bar represent the mean of the values ($\bar{X}(k) = \frac{1}{N}\sum_{k=0}^{N-1} X(k)$). First the standard variances D and the covariance C are needed: [3]

$$D_X = \frac{1}{N}\sum_{k=0}^{N-1}\left[X(k) - \bar{X}(k)\right]^2 \qquad D_Y = \frac{1}{N}\sum_{k=0}^{N-1}\left[Y(k) - \bar{Y}(k)\right]^2 \tag{2.4}$$

$$C_{XY} = \frac{1}{N}\sum_{k=0}^{N-1}\left(\left[X(k) - \bar{X}(k)\right] \times \left[Y(k) - \bar{Y}(k)\right]\right) \tag{2.5}$$

The normalization covariance factor (correlation) in equation 2.6 leads to the relative factor R_{XY} in equation 2.7.

$$LR_{XY} = C_{XY}/\sqrt{D_X D_Y} \tag{2.6}$$

$$R_{XY} = -\log_{10}(1 - LR_{XY}) \tag{2.7}$$

Power transformer measurements have defined threshold values for different levels of winding deformation, which, to a certain extent, can be an orientation for the faults in rotating machines. Therefore, the SFRA curve of a power transformer is divided into a low, medium and high frequency band. [3]

The relative factors of the certain frequency bands (R_{LF}: 1 kHz $\sim$ 100 kHz, R_{MF}: 100 kHz $\sim$ 600 kHz and R_{HF}: 600 kHz $\sim$ 1 MHz) and their values for the levels of deformation are represented in table 2.1.

The high sensitivity of the test also implies the susceptibility to environmental influences and thus requires a strict and precise procedure to minimize this impact. The IEC Standard 60076-18 recommends separate coaxial measurement leads of equal length for the source, response and reference connection and cable shields that are connected individually to the grounded chassis of the DUT. [18]

Winding Deformation Degree	Relative factors
Severe Deformation	$R_{LF} < 0.6$
Obvious Deformation	$0.6 \leq R_{LF} < 1.0$ or $R_{MF} < 0.6$
Slight Deformation	$1.0 \leq R_{LF} < 2.0$ or $0.6 \leq R_{MF} < 1.0$
Normal Winding	$R_{LF} \geq 2.0$, $R_{MF} \geq 1.0$ and $R_{HF} \geq 0.6$

Table 2.1: Threshold values for winding deformation. [3]

2.2 Impulse Frequency Response Analysis

A widely used method to examine the condition of stator windings is the impulse frequency response analysis (IFRA). A high voltage impulse is injected in one input terminal of the DUT, while the output terminal is on the same potential (ground potential or close to ground potential) as the chassis of the DUT and the backend of the impulse winding tester (IWT). The capacitor of the IWT and the inductance and capacitance of the DUT form a damped LC circuit. The measured voltage at the input terminal versus time gives the surge test the waveform of a damped oscillation. A simplified sketch of an IWT and the working principle can be seen in figure 2.2. [16] Equal to the SFRA method just illustrated, the form of the measured curve depends on the unique characteristics of the tested winding, equivalent to a signature or fingerprint.

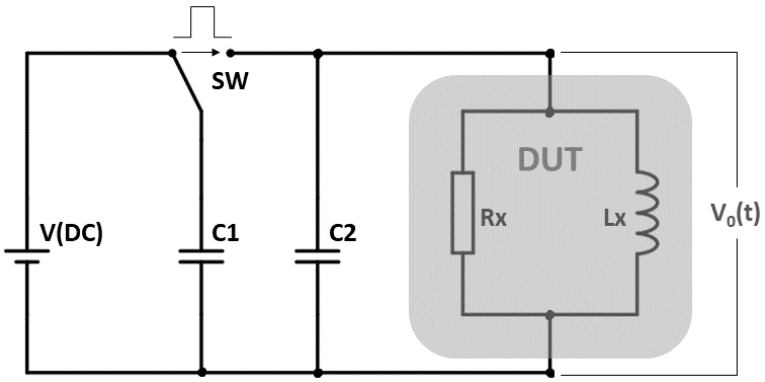

Figure 2.2: Simplified principle of an IFRA test. $C1$ is charged by the DC source and as soon as SW switches, the impulse discharges into the damped LC circuit, formed by $C1$, $C2$ and the DUT. The voltage versus time ($V_0(t)$) is recorded by either the IWT itself or an auxillary device like an oscilloscope.

The amplitude of the voltage impulse depends on the rated voltage U_n of the machine. An important precondition for the repeatability is of course the detailed documentation of the amplitude and the settings, to obtain feasible and comparable results.

The rapid rise of the impulse induces a higher turn-to-turn voltage at the input side than at the grounded output side of the winding, hence the voltage distribution is not linear. [16] Furthermore, the high frequencies of the signal are damped faster, and therefore filtered. [22] Consequently, the result also depends on the measurement direction, i.e. the same fault looks different if input and output terminal are switched.

2.2.1 Quantifying Results

Two IFRA measurements can be compared by various methods, and it takes some calculation to achieve the desired results. The evaluation (of one of the three following subsections) of the measured data is often done automatically by the IWT itself with an algorithm unknown to the user. Then the result of the test is just given as *FAIL* or *PASS* for the selected setting. For more differentiated conclusions, the following quantifying methods are determined separately with an additional measuring setup, in the case of this thesis, an oscilloscope (3.2.2) and a python script. The python code used can be found at `https://github.com/lukasdiem/waveform-comparison`. Note that in all three methods the curves are always compared in a defined range (A-B in the following graphics), never on the full range.

Absolute Area Size Comparison

The first quantifying method compares the absolute area of the two measurements (figure 2.3). Both areas, i.e. the area between the x-axis and the tested waveform, as well as the area between the x-axis and the reference waveform, are calculated. Then the difference of the areas is divided by the area of the reference waveform, which gives the similarity, expressed as a percentage value. [17]

The size of the area is proportional to the loss of energy in the winding. Inter-turn faults increase the energy loss and can thus be detected with this method. [20]

Differential Area Comparison

The differential area comparison (figure 2.4) calculates the area between tested and reference waveform and divides the result by the absolute area size of the reference curve. The result, expressed as a percentage, indicates the size of the deviation of the current test. [17]

This method reveals the change of inductance and the total loss of energy. Especially deviations of the machine's inductance can be detected with this comparison method. [20]

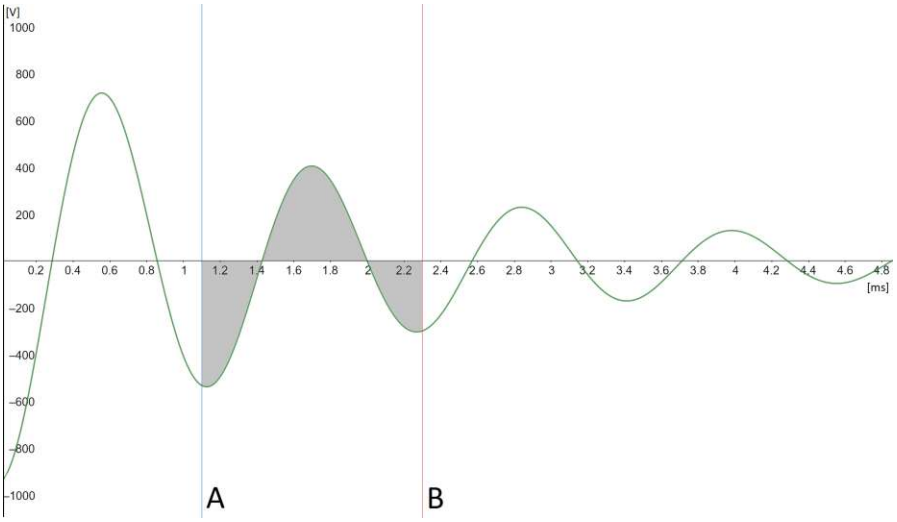

Figure 2.3: Calculation of the absolute area size, i.e. the area between curve and x-axis: The difference of the areas of the current test and the reference test is divided by the reference area and leads to a percentage value, which indicates the similarity of the waveforms.

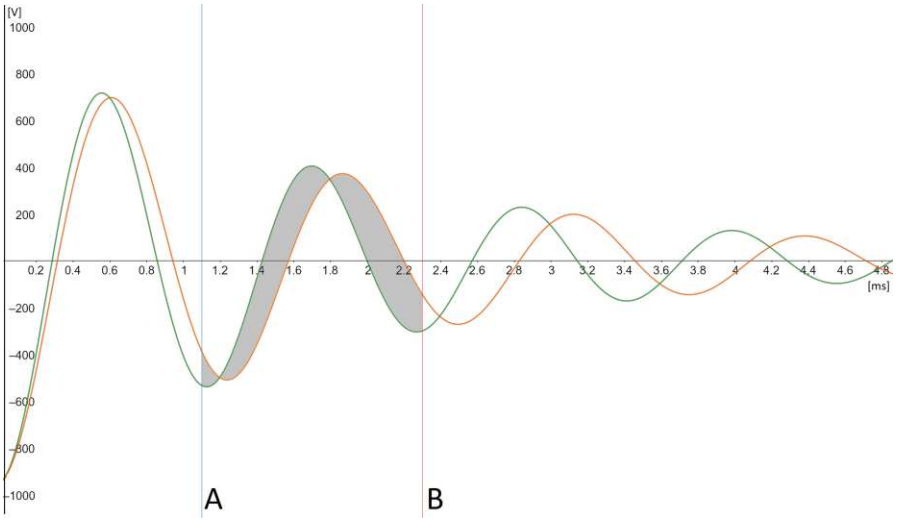

Figure 2.4: The differential area comparison calculates the area between the curves divided by the absolute area of the reference curve. The resulting percentage indicates the loss of inductance and energy.

Zero Point Comparison

Comparing the zero points (figure 2.5) of the tested and the reference waveform reveals the change of the LC circuit's resonant frequency. The larger the offset of the zero crossings (ZC), the bigger the frequency deviation, caused by a shift in inductance or capacitance. [17]

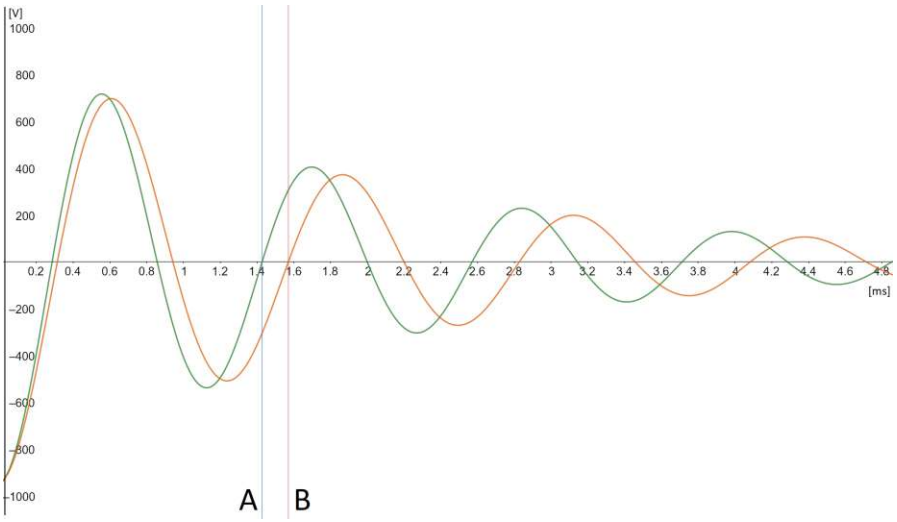

Figure 2.5: Comparing the zero crossings (here the third ZC) of the tested and the reference waveform shows the change of the resonance frequency.

Note that the ZC 1 (A and B are ZC 3 of each curve) cannot be used for this method since the first ZC does not reflect the actual behavior of the tested winding. [20]

3 Experimental Setup

The three tested and modified stators from *ELIN Motoren* are shown in figure 3.1. First, the six terminals (two per phase) of each stator are attached to the wooden framework above the stator in the middle, to avoid measurement variance caused by movement or rearrangement of the leads. Second, parts of the winding head are uncovered to gain access to the leads of one phase. Third, to simulate inter-turn or inter-winding faults, access points are soldered to single turns of the winding.

3.1 Stators

The physical properties of the stators are given in table 3.1. All of them have a few things in common:

- three individually accessible phases (denominated as U, V and W),
- concentric windings,
- random-wound windings,
- each phase has multiple parallel circuits,
- four poles,
- and 48 slots.

From now on, the stators in figure 3.1, from left to right, refer to *stator 1, 2* and *3*. *Stator 1* and *stator 3* have the same winding structure and diameters and differ physically only in their core length. *Stator 2* has different dimensions and another winding structure. Their impedances and specifications are shown in table 3.1.

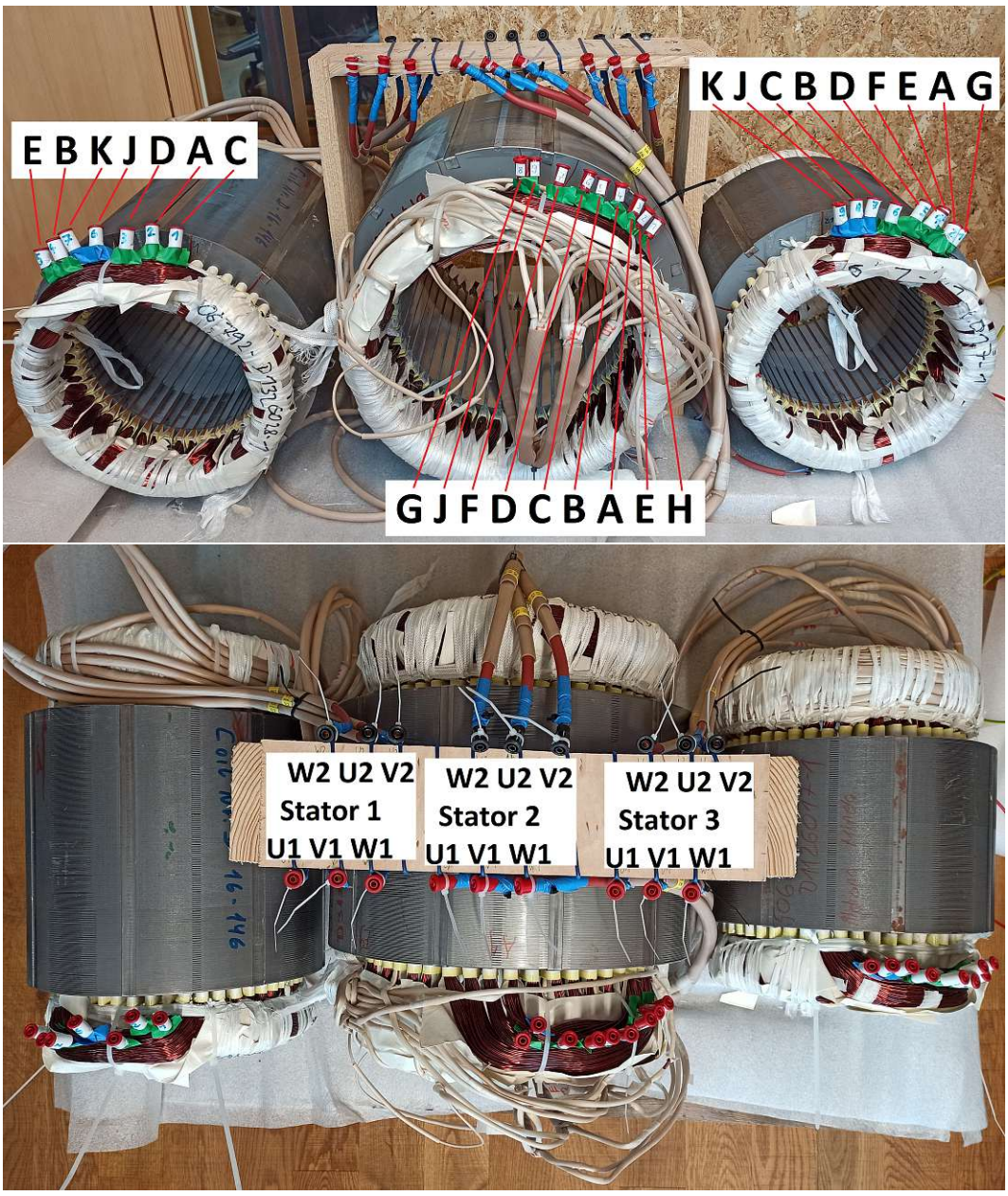

Figure 3.1: The three tested stators (1-3 from left to right): All phase terminals (U, V and W) are attached to the wooden framework to avoid movement of the leads. At the winding head, each stator has seven to nine access points (A-K) soldered to one phase to simulate inter-turn and inter-winding faults.

	Stator 1	*Stator 2*	*Stator 3*
Outer diameter [cm]	31.5	40	31.5
Inner diameter [cm]	19.5	25.5	19.5
Lamination core length [cm]	28	25	19
Resistance [mΩ]			
U1-U2	307.2	36.9	257.1
V1-V2	308.0	40.3	257.4
W1-W2	307.4	35.0	257.2
Inductance [μH]			
U1-U2	9031	831.3	6668
V1-V2	8880	815.1	6516
W1-W2	8958	812.4	6598
U_n [V]	480	380	400
I_n [A]	65	202	55
P [kW]	37	100	26

Table 3.1: Properties, resistances, inductances and specifications of the tested stators.

3.1.1 Winding Structure

The exact winding structure of all stators is known but cannot be published in full due to corporate secrets. *Stator 1* and *stator 3* have a single-layer winding structure with two windings per phase, each split into two coils (shown in figure 3.2).

Each phase of *stator 2* is built up of four parallel concentric windings installed in two layers, i.e. there are two windings per slot (shown in figure 3.3).

The windings of *stator 1* and *stator 3* have fewer but longer (more turns) parallel circuits compared to *stator 2*, which has more but shorter (fewer turns) parallel circuits.

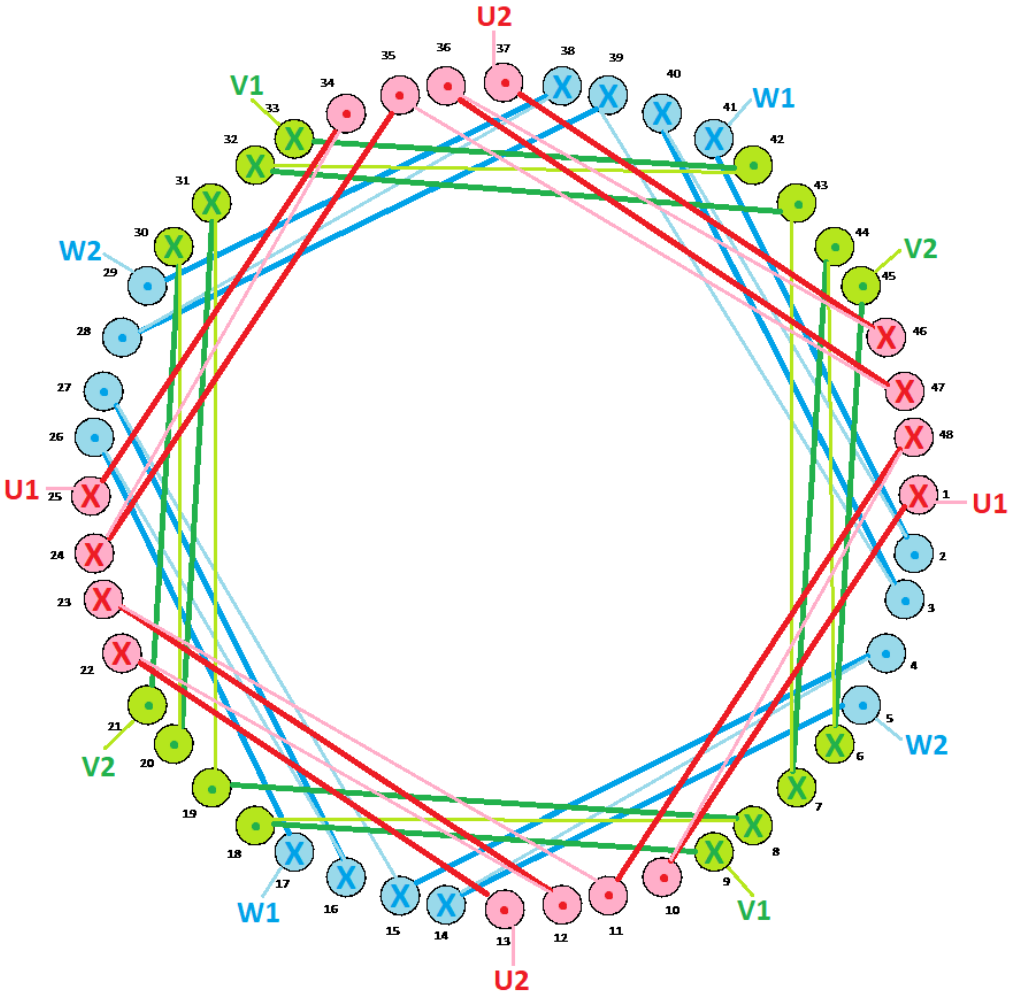

Figure 3.2: Single-layer winding structure of *stator 1* and *stator 3*: two windings per phase, split into two concentric coils (for example: winding 1-13 is split up between 11 and 12). The light colors indicate the connections between the winding parts. The access points of *stator 1* are installed in phase U in the winding part from slot 1 to 10, the access points of *stator 3* are also in phase U in the winding part from slot 22 to 13.

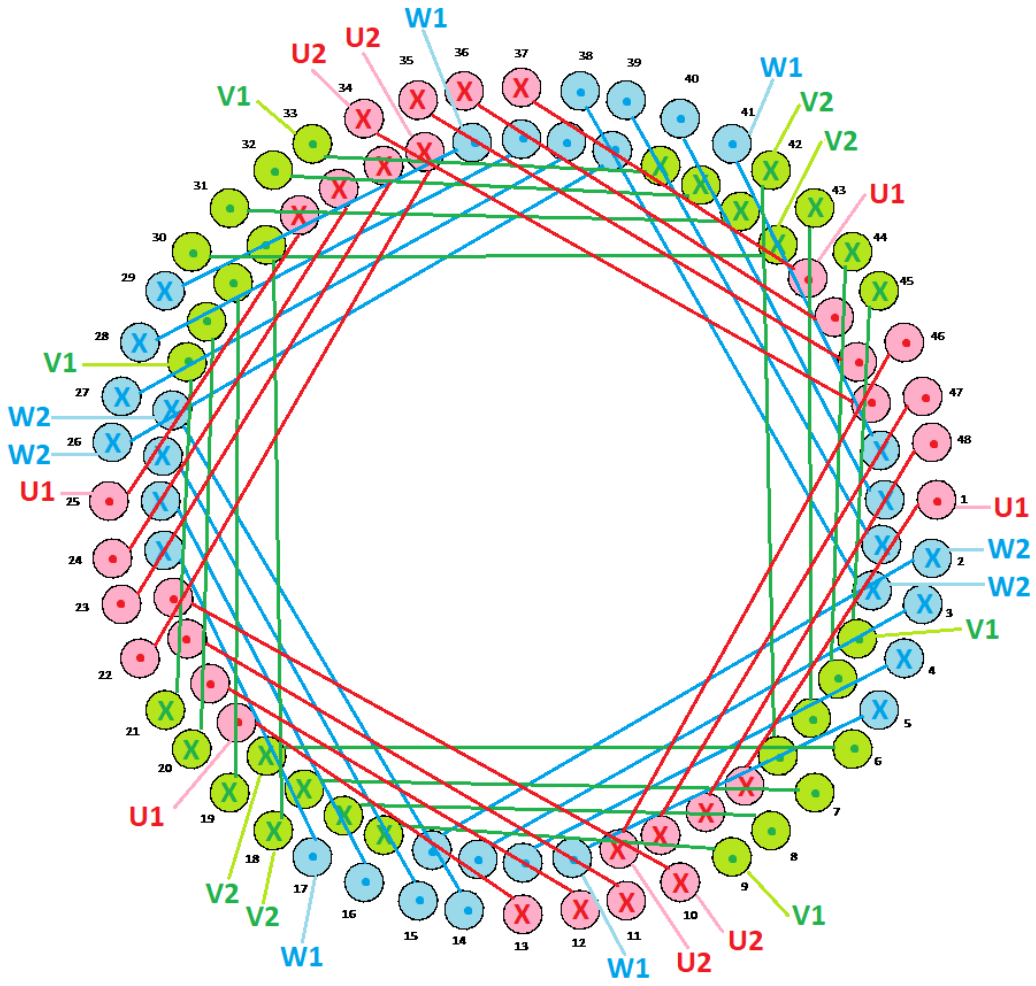

Figure 3.3: Double-layer winding structure of *stator 2*: Four concentric parallel windings per phase, integrated in an inner and outer layer, i.e. every slot contains two windings. The access points are installed in phase U between slot 1 and 8.

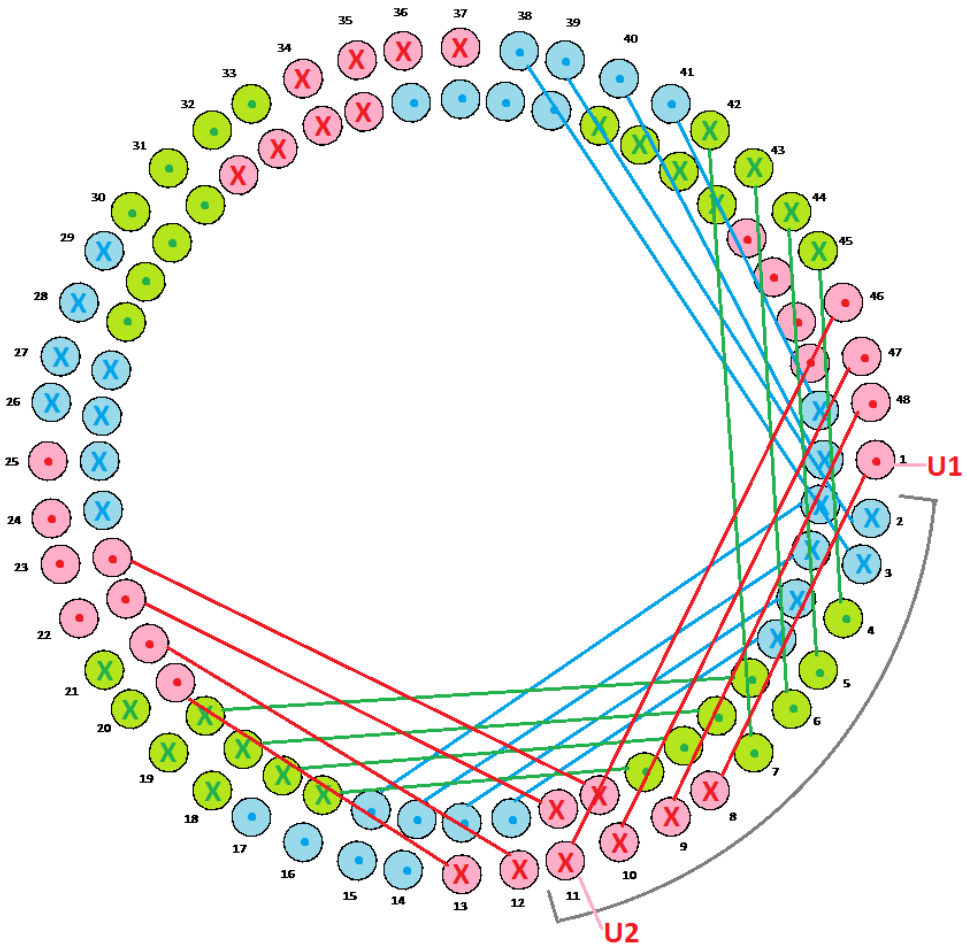

Figure 3.4: Actual winding structure of *stator 2*: The discrepancy is due to the manufacturing process. The part marked in gray differs from the theoretical winding structure in figure 3.3, the rest corresponds to it. The figure shows that the access points, installed between slot 1 to 8, are all in the outer layer.

3.1.2 Access Points of the Windings

To simulate different faults, predominantly inter-turn and inter-winding short circuits, access points are soldered to the wires between two chosen stator slots. All stators have one identifiable parallel circuit, so this one is chosen for the installation of the access points, to maximize the probability to mount two access points only one turn apart. Due to the random winding not all turns of one parallel circuit are reachable, and, therefore, only the accessible wires are used for manipulation. A few more access points are soldered to the wires of different parallel circuits in the same slot to simulate inter-winding circuits. For this task, it is necessary to work carefully to avoid the deformation of the winding, which would lead to a deviation of the measurement. The impact is evaluated with a measurement before and after the access point installation (figure 4.3 in the following chapter).

For all stators the adaptions are applied to the phase U, due to the ordinary random winding technology, where U is the phase placed first and, therefore, the outermost and most easily accessible winding. The access points of *stator 1* are in the winding part from slot 1 to 10, close to the $U1$ terminal, while *stator 3* has them between slot 22 and 13, close to $U2$ (figure 3.2). *Stator 2* has its access points in the winding placed in slot 1 and 8, close to $U1$, but note that the actual winding structure differs a little bit from figure 3.3. The difference is caused by the winding technology used, where the first inserted winding occupies 8 outer slot spots instead of theoretically 4 outer and 4 inner spots (shown in figure 3.4). Although this does not result in a disturbance of the measurement, it has to be mentioned.

3.2 Measuring Equipment

For satisfying SFRA measurements, several requirements have to be fulfilled. The coaxial cables used should be of the same length and kept short. Furthermore, the PE (protective earth) leads are kept tight, short and close to the device, just as recommended in the IEC standard 60076-18 [18]. All PE cables, i.e. the coaxial cable shields, the PE of the FRANEO 800 and the connection to the ground potential, are connected directly to a magnet, which is attached to the chassis of the stator currently being tested. The connection between magnet and stator was measured to ensure a negligible resistance. [4]

The IFRA measurement requires a slightly different setting. As well as for SFRA, the leads should be kept short to minimize their impact on the result. Unlike before, coaxial cables are not necessary and have no additional benefit. The chassis, the output terminal

of the tested winding and the ground potential are all connected to the aluminum band at the back end of the IWT.

To simulate different faults, a short cable connects two selected access points. For the comparison of SFRA and IFRA measurements, the access points used are always identical. All measurements are carried out with connection to the terminals $U1$, $V1$ or $W1$, and $U2$, $V2$ or $W2$ respectively, but never to the access points for the manipulation, since this configuration would have no relation to practice.

3.2.1 FRANEO 800

To record the SFRA signal of the stators, the device FRANEO 800, combined with the software *Primary Test Manager* (PTM) (both developed by *OMICRON*), was selected. The basic principle of the device is shown in figure 3.5 on the right. The measured parameter (the voltages $U1$ and $U2$) are transferred to the PTM software, which converts the data to a Bode-diagram.

[13]

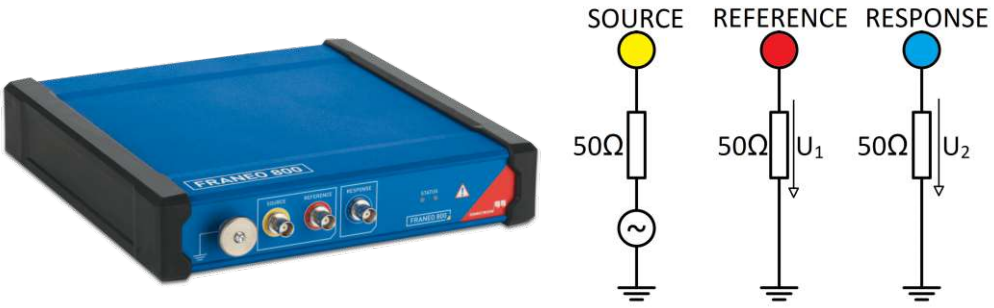

Figure 3.5: FRANEO 800: the left figure shows a picture of the device [11] and the right figure the corresponding setup and working principle.

The main properties from the technical data sheet are shown in table 3.2. The sensitivity errors of the FRANEO 800 fulfill the requirements of the standards of IEC 60076-18 [18] and IEEE C57.149 [1].

FRANEO 800	Amplitude	Frequency	Voltage
Range:	+10 dB to −140 dB	1 Hz to 30 MHz	0.1 V to 10 V

Table 3.2: Technical data of the FRANEO 800. [10]

To minimize the impact of the cables (source, reference and response), firstly, all of them must have the same length and properties. Secondly, the source and response cable

connect at the input terminal of the DUT and not before. The response cable is always attached to the output terminal of the same winding to provide a direct connection, capacitive measurements are not executed (figure 3.6). Every frequency applied to the DUT is held for several periods to grant a precise amplitude and phase value, before the next frequency is measured. The default settings for the measurements are set to 10 V and a frequency range of 20 Hz to 2 MHz, which corresponds to the standards mentioned before.

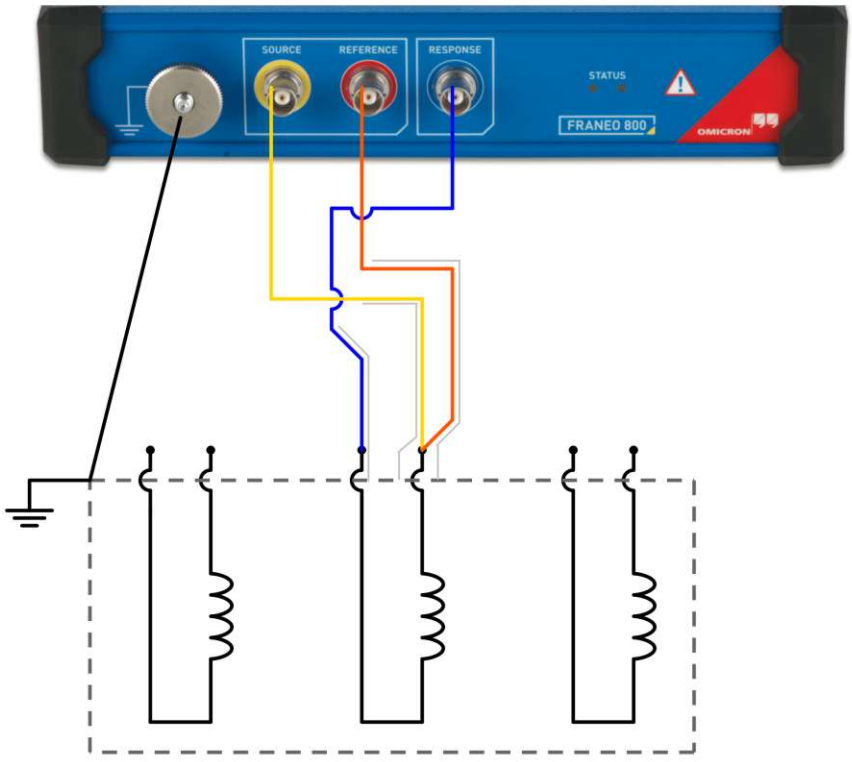

Figure 3.6: SFRA setup for testing a single phase of the stator. The gray lines symbolize the coaxial cable shields, which are connected to the chassis.

3.2.2 Sourcetronic Impulse Winding Tester

The IFRA measurements are carried out with the IWT ST2883-5 from *Sourcetronic* (figure 3.7). The working principle corresponds to figure 2.2 in the theory chapter, and the properties are given in table 3.3.

An impulse of 1000 V was chosen for the impulse test since this voltage is common practice for induction motors in this rated voltage range.

Output impulse voltage	0.1 kV to 5 kV
Inductance test range	>10 µH
Impulse energy	max. 250 mJ

Table 3.3: Technical data of the IWT ST2883-5. [17]

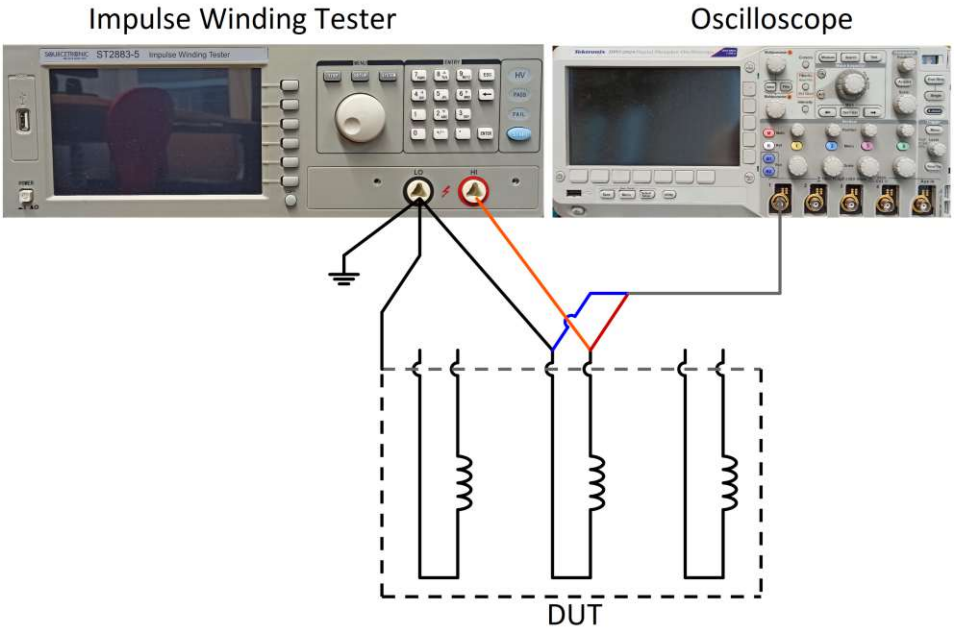

Figure 3.7: IFRA setup for testing a single phase of the stator.

Tektronix Oscilloscope

The setup of the surge test remains a regular IFRA measurement setup but the waveform is additionally recorded with an oscilloscope to enable the processing and comparison of different IFRA measurements (figure 3.7).

The oscilloscope is connected to the DUT with a 1 MΩ input-impedance at the port of the oscilloscope. Since the cable connecting the oscilloscope with the DUT is much smaller than one fourth of the wavelength (cable length $\ll \lambda/4$), the reflection of the electromagnetic wave does not have an appreciable impact on the measurement.

The data is analyzed with the python code accessible at `https://github.com/lukasdiem/waveform-comparison`. Furthermore, the data is smoothed with a Savitzky-Golay filter of third order for better comparison.

The sampling rate is set to the maximum of 200 GHz, and 1 million points are recorded. [19] The trigger is set to *impulse* with negative polarity and an impulse width larger than 1.5 µs.

4 Results and Discussion

The different cases and faults are evaluated with SFRA and IFRA and the findings compared to each other.

The IFRA evaluation frame contains three periods, beginning at the global maximum and ending at the third peak of the reference waveform (figure 4.2). The scale of the x-axis in the plots differs between the stators since their waveforms have different damping rates and frequencies and consequently have differing ranges of interest.

The information contained in a SFRA plot can best be visualized with a Bode-diagram, consisting of an amplitude-versus-frequency and phase-versus-frequency curve. The x-axis, i.e. the frequency, is usually shown in a logarithmic scale to provide a decent representation of the findings. The y-axis of the phase curve is limited from $-180°$ to $180°$. For larger phase changes, the plot jumps to the opposite, recognizable at the vertical lines (saltus).

The following SFRA plots do not always show the complete range measured, mostly they focus on the interesting frequency range, which can also differ depending on the investigated stator.

4.1 Settings

The threshold values used to identify a fault case are defined during the process of the measurements and base on the gained experience.

The IFRA comparison of the healthy phases usually show a deviation around 5% for the area size and differential area evaluation, while almost all fault cases have more than 10% deviation for both quantifying methods. Thus the IFRA fault condition was set to >10% for area size **and** differential area comparison. This criterion shows the advantage of the computer-assisted calculation, where both values can be calculated from one measurement, contrary to the IWT integrated software, which can only evaluate one quantification method at once. The zero crossing comparison was neglected since it could not provide any additional information during this measurement series.

The fault criterions for SFRA are evaluated below 200 kHz since the frequency range above did not provide any further information about the winding's condition or improvement of the fault detection for these particular stators. The criterions are, on the one hand, the relative factor R_{LF} in the frequency range below 100 kHz. R_{LF} is not evaluated up to 200 kHz since the software allows the evaluation only in certain ranges, which could not be adjusted. The chosen threshold is the same as for power transformers, i.e. $R_{LF} < 2$ (table 2.1). On the other hand, faults are often obvious in the Bode-diagrams: The *amplitude gap* condition describes the shift of the amplitude trend, and the displacement of a peak is denominated as the *resonance shift* condition (often visible in the phase plot). For the SFRA fault detection one fulfilled criteria is enough for the diagnosis, unlike the IFRA tests, where both have to be fulfilled.

Access Points

To identify the exact turn each access point is soldered to, the resistances between all access points and terminals (U_1 and U_2) are measured with the four point method. The results for each stator are measured with a *CPC 100* from *OMICRON* and shown in table 4.2, 4.3 and 4.4. [12]

The resistance values lead to the order of the access points (table 4.1). Note that the smaller the turn number, the closer the turn is to the nearest phase terminal (U_1 or U_2), i.e. the turn numbering starts at U_1 for *stator 1* and *2*, for *stator 3* it starts at U_2.

Stator 1		*Stator 2*		*Stator 3*	
access point	turn number	access point	turn number	access point	turn number
A	1	A	1	A	1
B	3	B	2	B	7
C	4	C	3	C	8
D	5	D	4	D	15
E	6	E	5	E	16
		F	6	F	17
J	sym to A	G	10	G	28
K	sym to A	H	11		
				J	sym to A
		J	sym to G	K	29

Table 4.1: Positions of the access points: A-H are located in one single parallel circuit, J and K are located in other parallel circuits in the same slot. "sym to A" means symmetric to access point A.

AP	A	D	B	E	J	K	U1	U2
C	40.37	15.61	14.16	28.89	62.81	63.01	52.24	336.6
A		52.97	29.05	65.73	24.98	25.19	14.23	312.7
D			27.15	15.67	75.29	75.4	64.68	343.9
B				40.35	51.64	51.68	41.15	329.6
E					88.29	88.31	77.57	352.2
J						26.97	16.02	314.7
K							15.87	314.6

Table 4.2: Resistance values between the access points and terminals of *stator 1* in mΩ.

AP	E	A	B	C	D	F	G	J	U1	U2
H	74.84	113.7	104.5	94.79	84.56	62.78	13.66	224	125	144.2
E		52.96	40.62	27.68	14.24	16.46	65.64	168.7	68.28	94.59
A			15.49	29.02	41.91	65.43	106.1	120.6	19.35	50.62
B				15.66	29.1	53.6	96.46	133.6	32.75	62.68
C					15.64	41.24	86.27	146.3	45.62	74.2
D						28.43	75.62	158.2	57.85	85.1
F							52.94	179.8	79.92	104.7
G								217	118	137.9
J									104.6	124.3

Table 4.3: Resistance values between the access points and terminals of *stator 2* in mΩ.

AP	A	E	F	D	B	C	J	K	U1	U2
G	231.9	126	117.4	135.1	193.4	185.4	471.1	251.2	391.1	240.2
A		128.9	138.1	120.6	54.62	64.71	262.5	24.48	262.1	12.92
E			12.01	11.73	81.63	71.86	378.8	150.2	338.2	138.9
F				22.3	91.35	81.71	387.1	159	343.4	147.8
D					72.64	62.8	371.4	142.1	333.8	130.5
B						12.97	311.6	77.21	294.8	65.64
C							320.5	86.84	301.3	75.34
J								265.5	411.6	254.5
K									264.4	15.69

Table 4.4: Resistance values between the access points and terminals of *stator 3* in mΩ.

Directionality

Figure 4.1 shows the impact of the measurement direction on the SFRA process. In both cases, fault-free and single inter-turn fault, the deviations of the course of the curve is negligible compared to the differences between a fault-free and an inter-turn fault measurement.

The IFRA tests in figure 4.2 reveal the high dependency on the position of the fault (in the perspective of the input terminal). While the fault-free case has no noteworthy differences, the inter-turn fault curves clearly show a frequency rise of the red waveform.

All the following measurements are executed with $U1$, $V1$ or $W1$ as input terminals, if not explicitly mentioned otherwise.

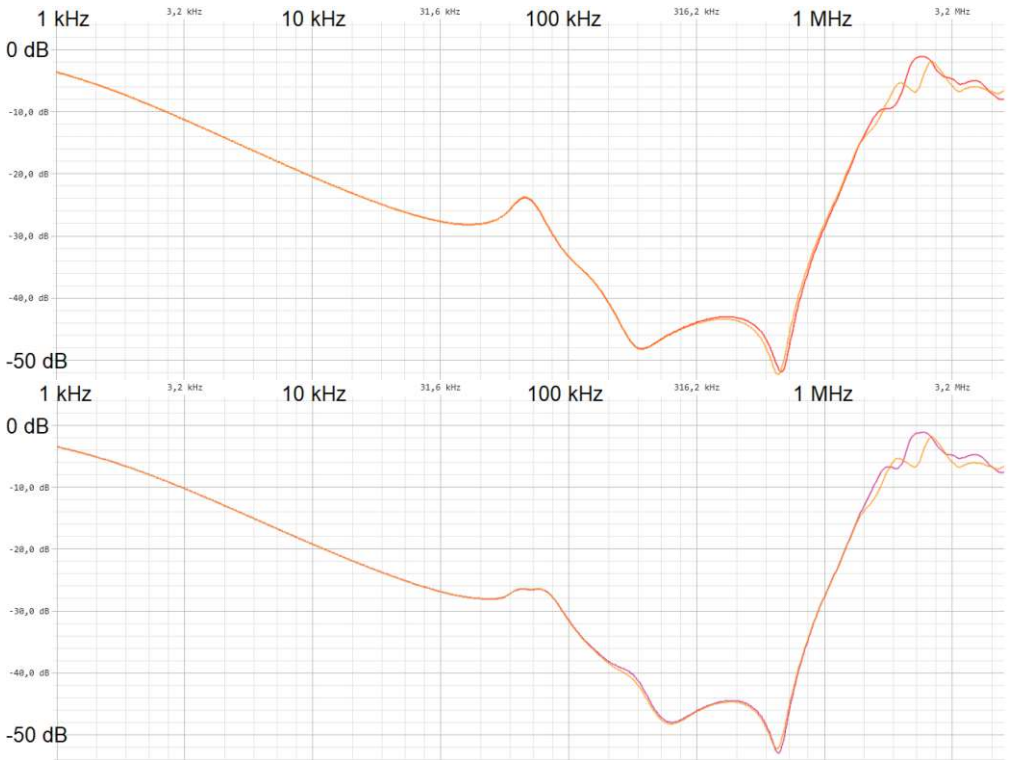

Figure 4.1: *Stator 1*, Phase U: The upper plot shows the fault-free case, the lower plot an inter-turn fault between access point C and D (i.e. a single turn is short-circuited, table 4.1). In both figures, the red curve represents the test with $U1$ as input terminal. The orange one was recorded with $U2$ as input terminal.

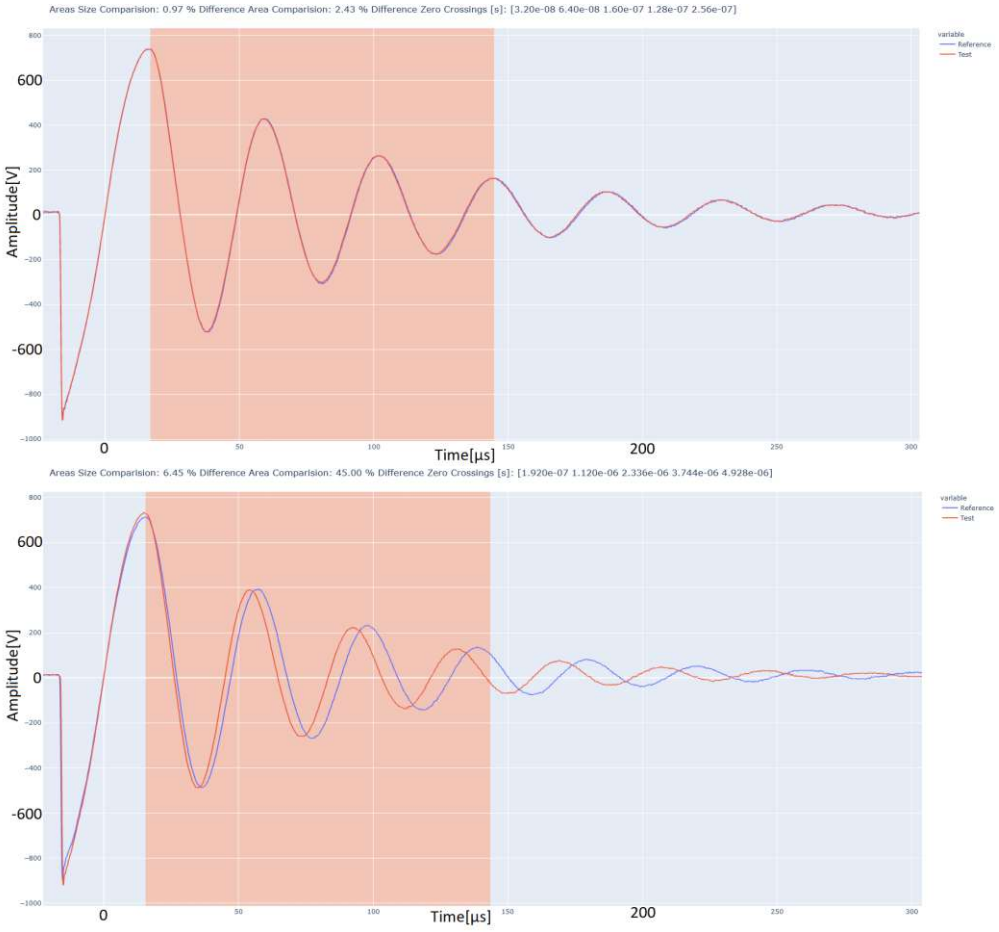

Figure 4.2: *Stator 1*, Phase U: The upper plot shows the fault-free case, the lower plot an inter-turn fault between access point B and C (i.e. a single turn is short-circuited, table 4.1). In both figures, the blue curve represents the test with $U1$ as input terminal, the red one with $U2$ as input terminal. As mentioned in section 3.1.2, the fault in this case is close to $U1$.

Repeatability

The repeatability measurement in figure 4.3 shows, on the one side the impact of the access points, on the other side the factor of time. The second factor is informative only to a limited extent since the time period between the measurements was only two weeks. Furthermore, the stators were obviously not in operation, and the environmental influence of an air-conditioned office is close to zero (i.e. barely any changes in temperature and humidity). Nevertheless, it shows the generally high repeatability of the SFRA process.

Figure 4.3: *Stator 3*, Phase U: Comparison of the frequency response before (orange) and after (red) the access point installation (cutting the winding head open and soldering the access points) of the stator.

Figure 4.4: *Stator 2*, Phase U, single inter-turn faults: E-F (orange), G-H (purple), D-E (turquoise) and C-D (red).

Comparing specific faults (for example one short-circuited turn) at different positions in the winding should not make any difference to the SFRA measurement, according to section 4.1. Figure 4.4 confirms this assumption and shows nearly indistinguishable curves for four different single inter-turn faults of *stator 2*.

Figure 4.5 shows the comparison of two single inter-turn faults, measured with the IWT. Section 4.1 (dependency of the measurement direction) would let us suppose that the results should differ slightly, since the position of the fault has an impact. However, the waveforms are pretty similar (1.3% area size and 2.4% differential area) due to the fact that the inserted faults are only four turns apart. The discrepancy is slightly bigger than the single turn fault comparison of two measurements with only one turn apart (figure 4.6, 0.2% area size and 0.8% differential area) but definitely not significant. Considering the fact that the whole winding has multiple turns, compared to the few turns position difference, this effect cannot be large.

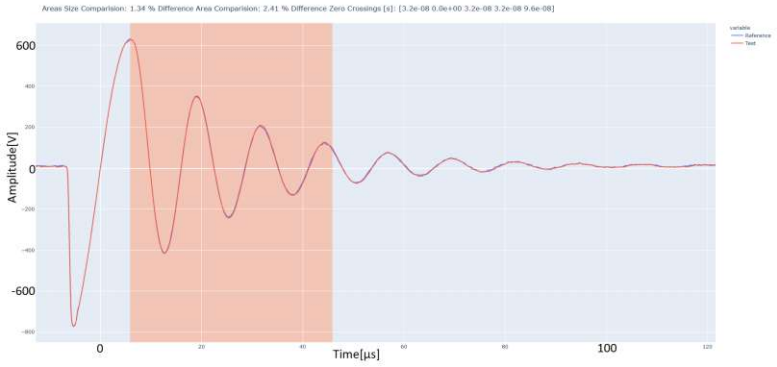

Figure 4.5: *Stator 2*, Phase U, single inter-turn faults: E-F (blue) and G-H (red).

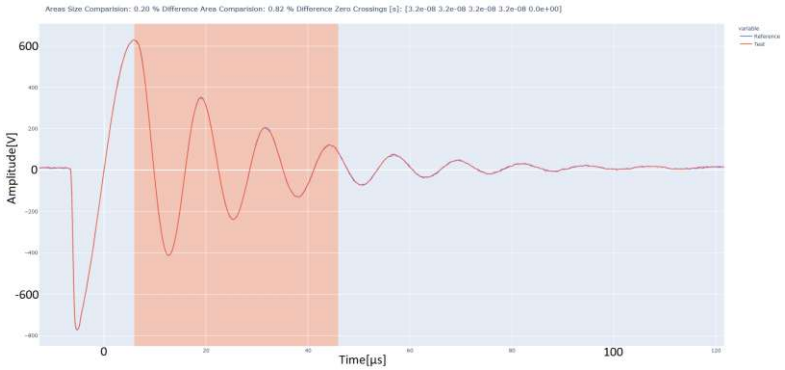

Figure 4.6: *Stator 2*, Phase U, single inter-turn faults: D-E (blue) and E-F (red).

Fault Impact on Non-directly Affected Phases

Figure 4.8 and 4.9 show the backcoupling of faults to other phases, V in this case. Phase V was measured once with no fault in U and once with a connected one turn short circuit in U (figure 4.7). No significant impact could be distinguished, neither with SFRA nor with IFRA.

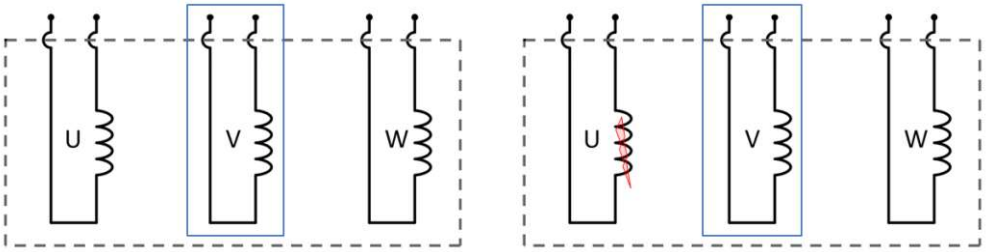

Figure 4.7: Measurement setup to determine the backcoupling of a fault.

Figure 4.8: *Stator 1*, Phase V: fault-free case (dark green) and one turn fault C-D in U (light green).

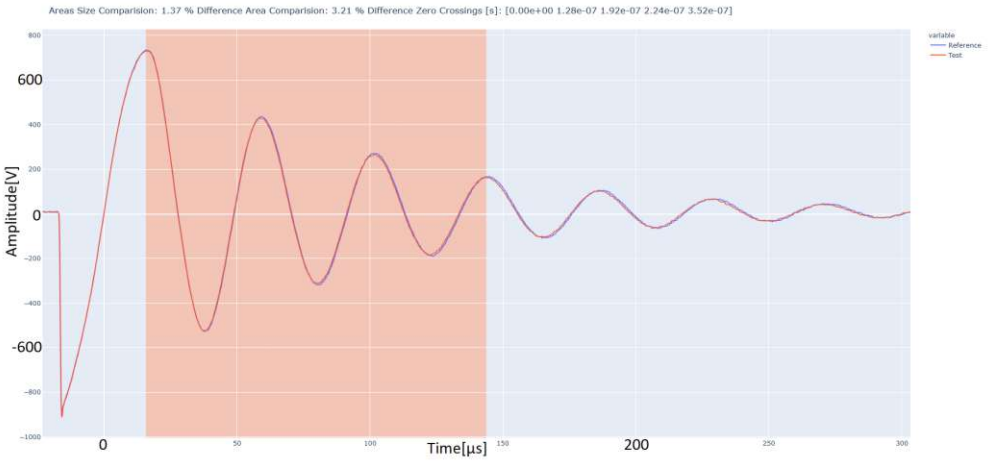

Figure 4.9: *Stator 1*, Phase V: fault-free case (blue) and one turn fault C-D in U (red).

Winding Structure Impact

The winding structure has a strong impact on the trend of the SFRA measurement. Obviously, there is an impact on the IFRA result as well, but there is no such thing as a characteristic waveform for different winding structures (figure 4.11), contrary to the SFRA measurement in figure 4.10, which leads to exactly this assumption.

Stator 1 and *stator 3* exhibit a distinct similarity, while *stator 2* differs strongly in all frequency ranges. The shift from the resonance frequencies of *stator 1* (the larger one) to the lower frequencies could be caused by the following: the larger cross section A of each winding leads to a higher inductance L ($L \propto N^2 A/l$; table 3.1). Simultaneously, the longer length of one turn enlarges the conductance C between the wires. Hence, the resonance frequency ($\propto 1/\sqrt{L \cdot C}$, for a resonant circuit) drops.

Note that the impedance view of the PTM software shows that the gap between *stator 1* and *stator 3* is larger, by orders of magnitude ($<$15 Ω), than just the resistance difference ($\sim$50 mΩ, table 3.1).

Figure 4.10: Phase U: *stator 1* (red), *stator 2* (light green), *stator 3* (orange).

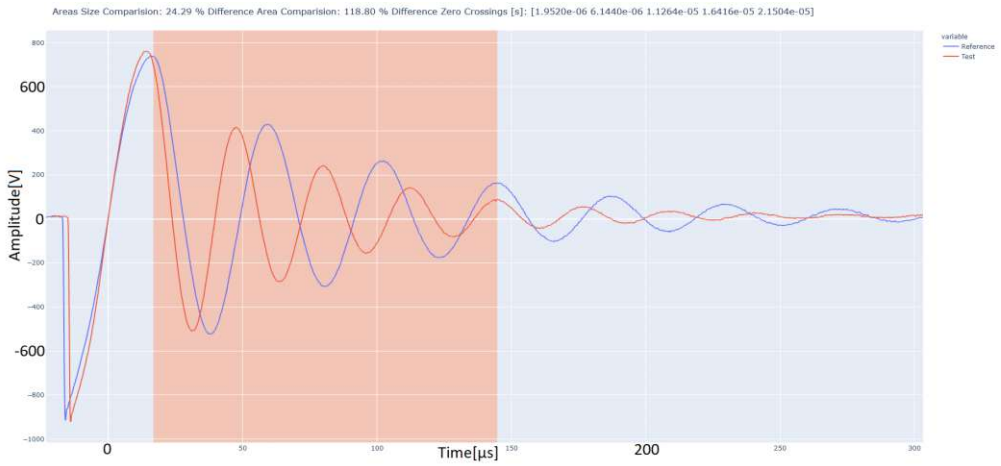

Figure 4.11: Phase U: *stator 1* (blue) and *stator 3* (red).

4.2 Inter-Turn Faults

Stator 3

The most common fault in stators is a short circuit between two turns of a winding. The comparison with a fingerprint measurement provides the clearest results to identify this maloperation (figure 4.12). On the one hand, the faults can be determined by the relative factor for the low frequency range R_{LF} (shown in table 4.5), on the other hand, they differ unambiguously from the fingerprint plot. Two typical visual signs can be determined, which indicate short-circuited turns: first, an amplitude gap below 40 kHz of a few dB and second, a shift of the resonance frequencies, observable at the saltus of the phase plot in the lower part of the Bode-diagram (around 120 kHz in figure 4.12). Both phenomena can be explained as a result of an inductance reduction, induced by at least one short-circuited turn.

Figure 4.13 illustrates the three healthy phases of *stator 3* and underlines their similarity, equal to the relative factors in table 4.5. Since there is not always a fingerprint available, phase comparisons also provide useful information about the winding's condition. The phase comparison in figure 4.14 clearly shows the amplitude gap between the fault and the healthy phases V and W, as well as the resonance shift in the phase plot.

If at least one of these three indicators (R_{LF}, amplitude gap, or resonance shift) under 200 kHz is distinguishable, there is most likely a short circuit in the tested winding.

		U	V	W
U		4.89	3.02	2.47
V		3.02	5.16	2.12
W		2.55	2.16	4.83
E-F	1t	1.77	1.99	1.46
D-F	2t	1.60	1.78	1.34
A-F	16t	1.39	1.53	1.19
A-G	27t	1.35	1.48	1.16

Table 4.5: Relative factors of the low frequency range R_{LF} (>100 kHz) of *stator 3*. The values are generated from the plots in figure 4.12 and 4.14, compared to the measurements before the access point installation. The first column represents the current results, the second column the amount of short-circuited turns, and the top line the fingerprint (measurement before access point installation).

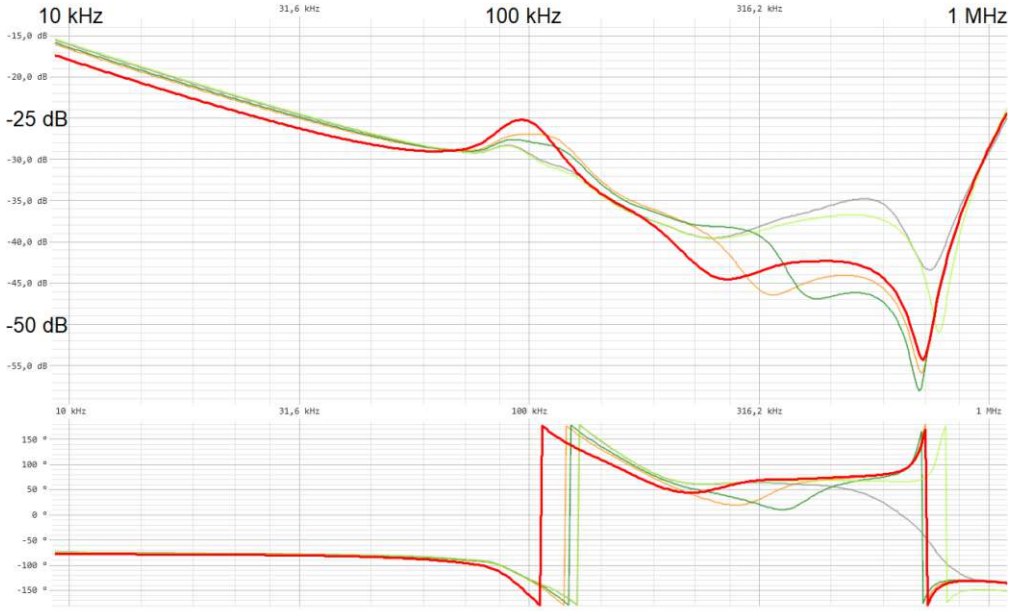

Figure 4.12: Fingerprint measurement (phase U) of *stator 3*: healthy fingerprint (red, thick), E-F (1 turn, orange), D-F (2 turns, dark green), A-F (16 turns, grey) and A-G (27 turns, light green).

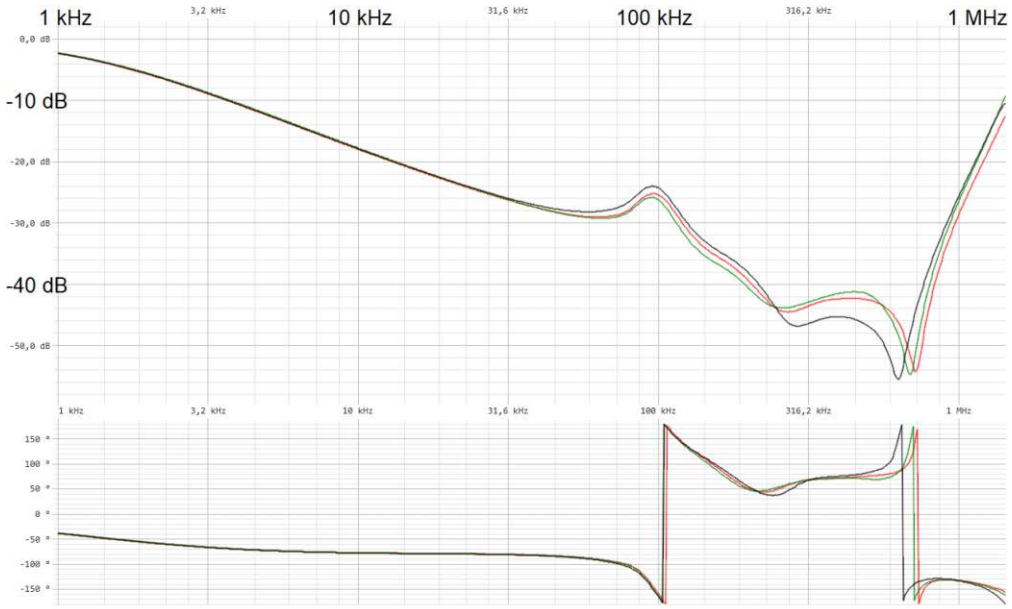

Figure 4.13: Phase U (red), V (green) and W (black) of *stator 3*.

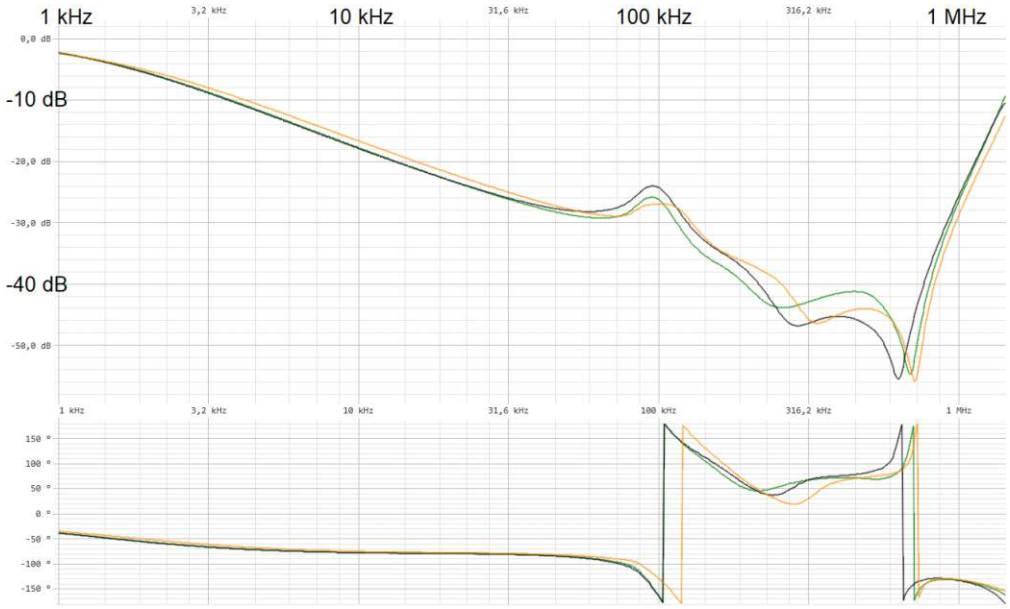

Figure 4.14: Phase comparison of *stator 3*: E-F (1 turn fault, orange), V (green) and W (black).

Stator 1

The single inter-turn fault C-D of *stator 1* in figure 4.15 is reliably identifiable by various indicators: first, the amplitude gap visible up to 30 kHz and the phase shift around 80 kHz. The fault is detectable by fingerprint comparison and phase to phase comparison.

The relative factors in table4.6 are smaller than 2 ant therefore indicate the faults reliably with both comparisons, fingerprint and phase to phase.

		U	V	W
U		3.92	3.82	2.17
V		3.70	4.57	2.16
W		2.35	2.27	4.68
C-D	1t	1.39	1.38	1.25

Table 4.6: Relative factors R_{LF} of *stator 1*. The values are generated from the plots in figure 4.15 and a measurement executed one day earlier. The first column represents the current results, the second column the amount of short-circuited turns, and the top line the comparison measurement.

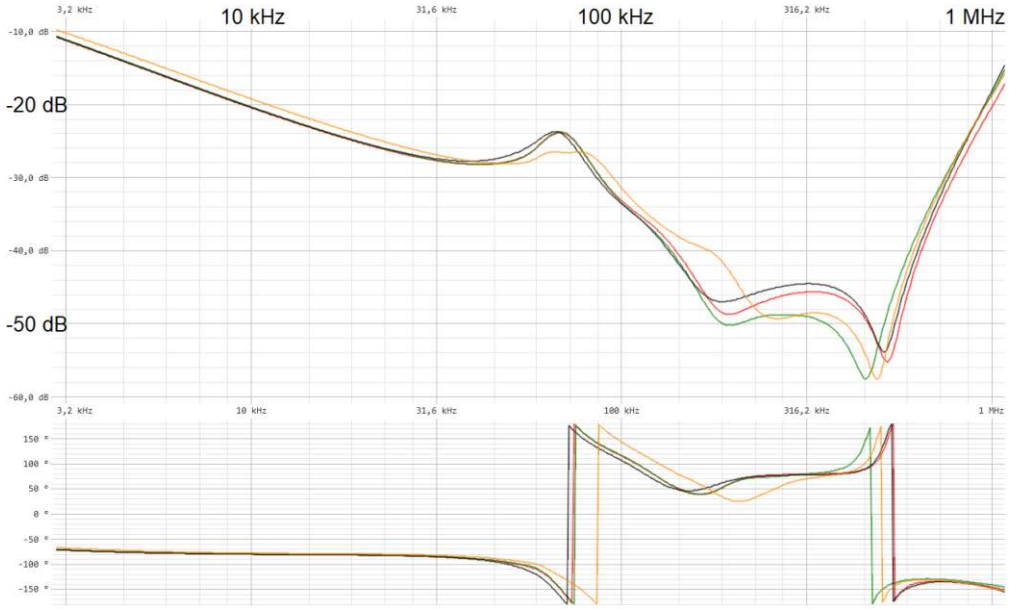

Figure 4.15: *Stator 1*: C-D (one-turn fault, orange), U (red), V (green) and W (black). The fault is clearly distinguishable by the gap in the amplitude and the frequency shift of the phase saltus.

Stator 2

The single inter-turn fault measurement of *stator 2* is shown in figure 4.16. The amplitude gap increases continuously up to 150 kHz. The shift of the saltus in the phase plot of the healthy phase U at roughly 400 kHz is out of the frequency range of interest and, thus, can be neglected.

The relative factors of *stator 2* in table 4.7 do not indicate a fault since all of them are larger than 2. However, they show the large similarity between the healthy phases.

Since one fulfilled fault condition determines a fault reliably, the single inter-turn fault E-F of *stator 2* can be identified by fingerprint and phase to phase comparison.

		U	V	W
U		7.46	4.56	4.37
V		4.52	8.18	5.79
W		4.35	5.73	8.46
E-F	1t	4.38	5.15	4.99

Table 4.7: Relative factors R_{LF} of *stator 2*. The values are generated from the plots in figure 4.16 and a measurement executed one day earlier. The first column represents the current results, the second column the amount of short-circuited turns, and the top line the comparison measurement.

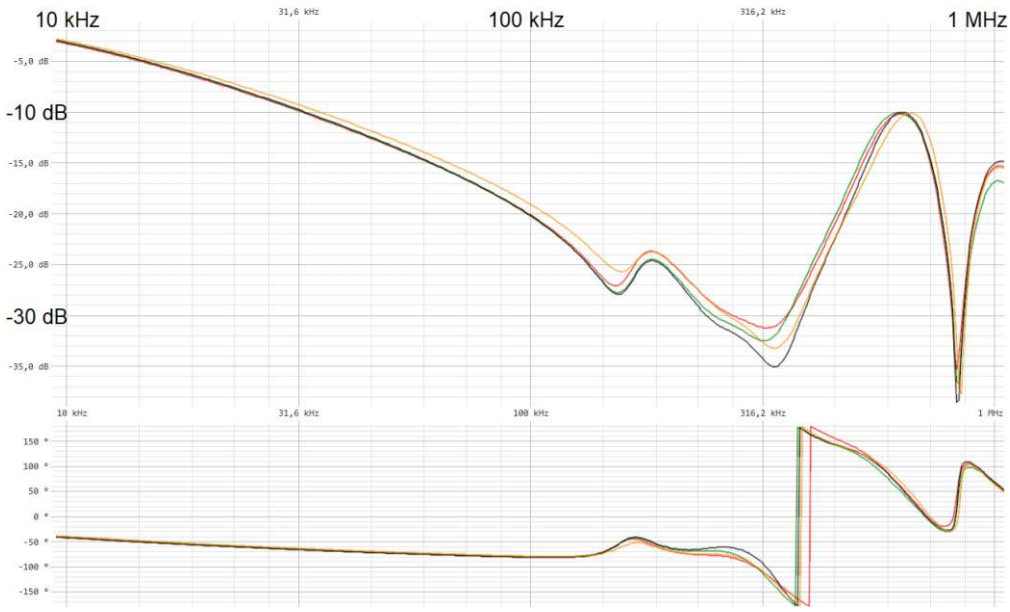

Figure 4.16: *Stator 2*: E-F (one-turn fault, orange), U (red), V (green) and W (black). The fault is clearly distinguishable by the gap in the amplitude.

Comparison with IFRA

The IFRA fingerprint measurement of *stator 3* is shown in figure 4.17. The area size and differential area value (17.8% and 77.8%) clearly identify the fault in the winding. The raise in the resonance frequency, caused most likely by the inductance drop, is identifiable. Comparing the healthy phases (figure 4.19) shows that a phase comparison is also informative. Their quantifying values are listed in table 4.8 and illustrate the necessity of fulfilling both fault conditions, just one value >10% does not indicate a fault. The same is shown in table 4.9 with the values of *stator 1* and *2*.

The slightly lower amplitude of the impulse measurement with an implied fault results from the reduced lead length, shortened by at least one turn. Intuitively, the voltage should rise since the length and thus the resistance is smaller, but this effect is canceled by the fact that the voltage distribution is now dropping faster (from 1 kV to 0 V on a length shorter by one turn than in the fault-free case). Hence, the voltage in the lead from the IWT to the DUT (figure 3.7) also drops further, and the recorded voltage at the input terminal is lower than in the fault-free case.

A single inter-turn fault compared to another phase (V, in this case) is shown in figure 4.18, and the fault can be identified as well. 20.8% area size difference and 78.2% differential area are above the thresholds of the fault condition.

Stator 3	*U-V*	*U-W*	*V-W*
Area size comparison	3.9%	1.1%	2.7%
Differential area comparison	5.0%	10.6%	8.8%

Table 4.8: Quantifying values of *stator 3*: comparison of the healthy phases (figure 4.19).

Stator 1	*U-V*	*U-W*	*V-W*
Area size comparison	2.0%	1.1%	0.8%
Differential area comparison	3.7%	13.6%	16.8 %
Stator 2	*U-V*	*U-W*	*V-W*
Area size comparison	1.0%	0.8%	0.2%
Differential area comparison	7.6%	2.1%	6.1 %

Table 4.9: Quantifying values of *stator 1* and *2*: comparison of the healthy phases.

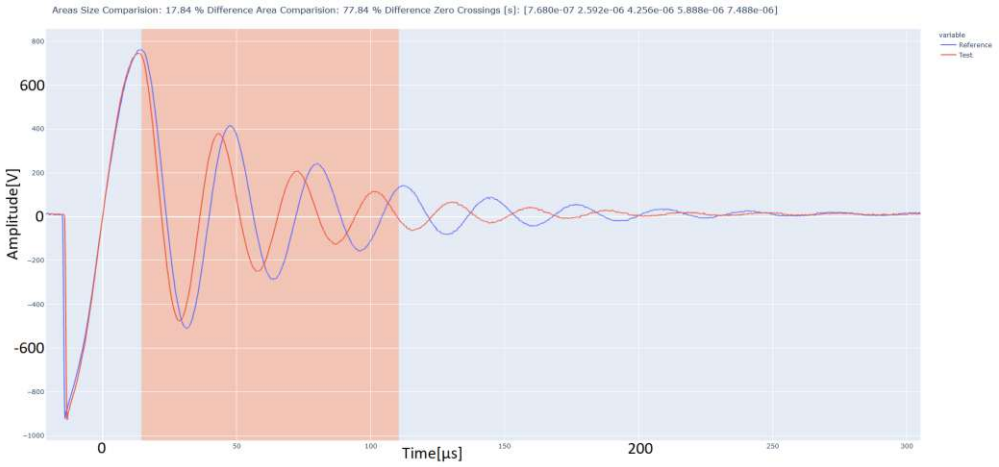

Figure 4.17: Fingerprint measurements of *stator 3*: healthy phase U (blue) and E-F (one turn fault, red).

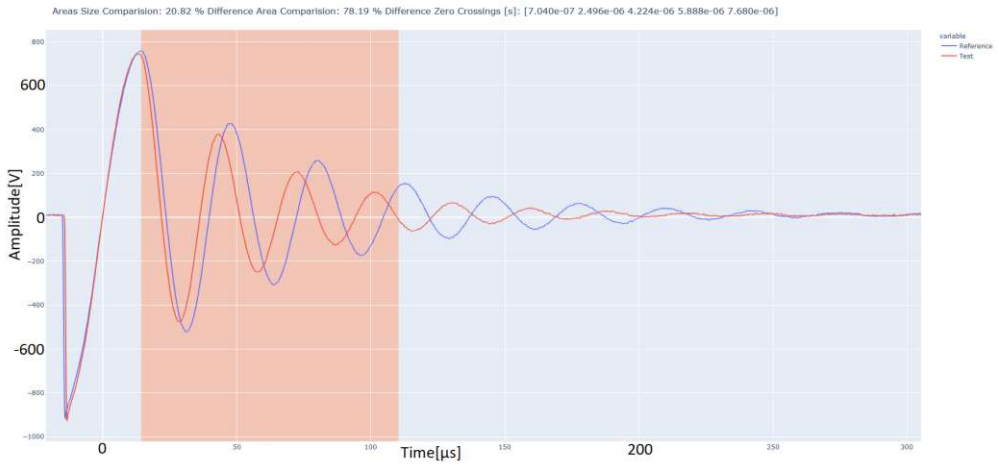

Figure 4.18: Phase comparison of *stator 3*: healthy phase V (blue) and E-F (one turn fault, red).

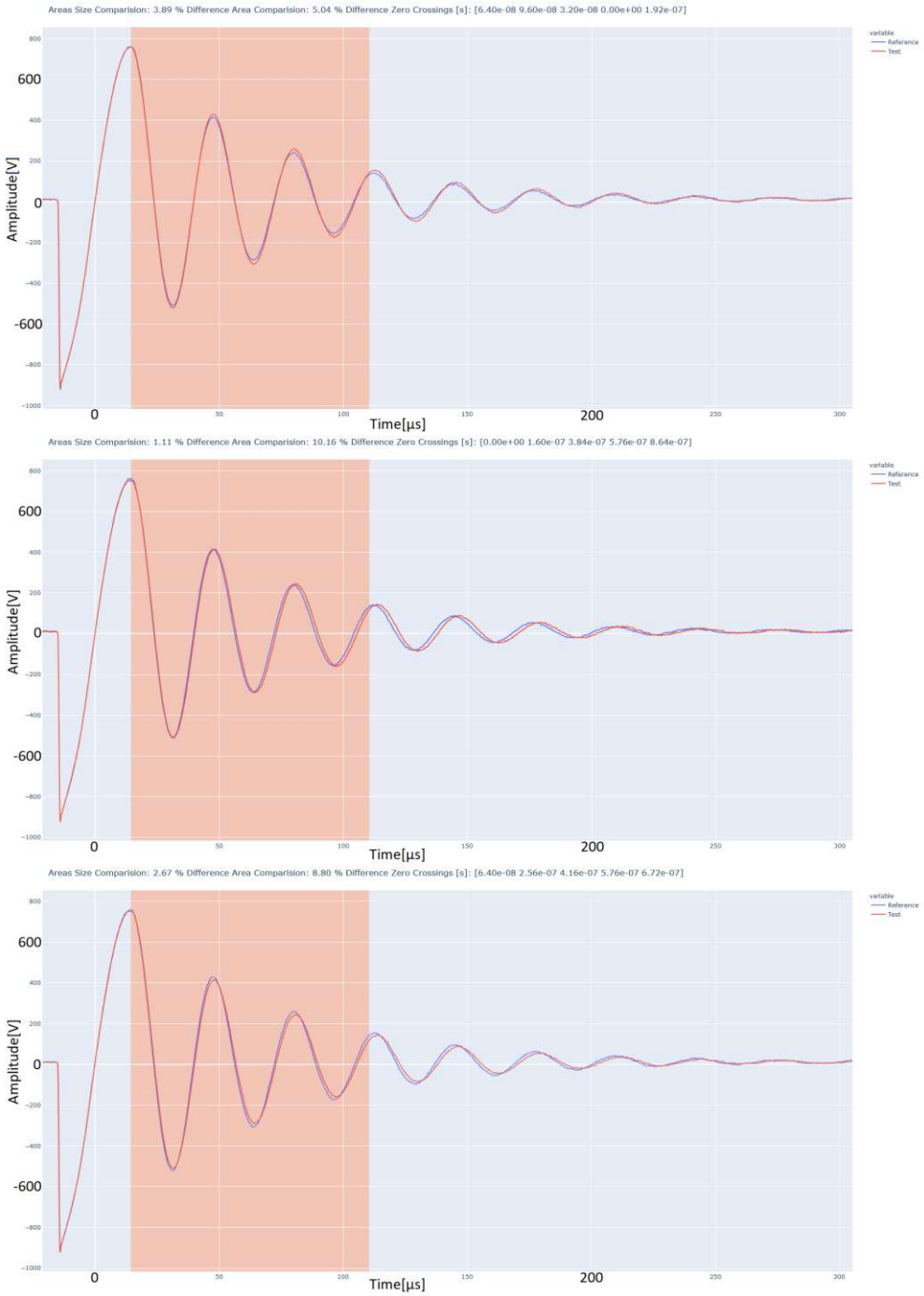

Figure 4.19: Phase comparison of *stator 3*: upper plot phase U and phase V (area size 3.9% and differential area 5.0%), middle plot U and W (1.1% and 10.6%), lower plot V and W (2.7% and 8.8%). The first phase mentioned is the reference (blue), the second one the compared waveform (red).

4.3 Inter-Winding Faults

Stator 2

In stators, multiple parallel windings can be placed in one slot. Usually, they are not specifically separated and inter-winding faults can thus also occur. Speaking of inter-winding faults means for the following results that two different parallel circuits of the same phase, both placed in the same slot, are short circuited. Inter-winding faults have to fulfill at least one of the three SFRA fault conditions to be identified. The SFRA measurement in figure 4.20 of *stator 2* shows the inter-winding faults compared to the fingerprint.

The 4-turn asymmetric fault (F-J) is determinable by fingerprint and shows two fault conditions, the amplitude gap and the resonance shift. Though the resonance shift appears above 200 kHz, it is still significant. The one-turn asymmetric case (H-J) is potentially identifiable with the fingerprint (small gap in the amplitude) but not with the phase comparison. The symmetric fault case (G-J), i.e. both windings are short-circuited after the same number of turns, is indistinguishable from the fingerprint. The relative factors in table 4.10 are not below the threshold but show a decline for an increasing number of short-circuited turns. The waveform of the detectable inter-winding faults strongly resemble the inter-turn faults, e. g. the single inter-turn fault E-F and the 4-turn asymmetric inter-winding fault F-J in figure 4.20.

		U	V	W
G-J	0t	4.65	4.55	4.37
H-J	1t	6.56	4.60	4.41
F-J	4t	4.75	5.11	4.80

Table 4.10: Relative factors of the low frequency range R_{LF} of *stator 2*. The values are generated from the plots in figure 4.20. The first column represents the current results, the second column the amount of short-circuited turns, and the top line the comparison measurement recorded one day earlier.

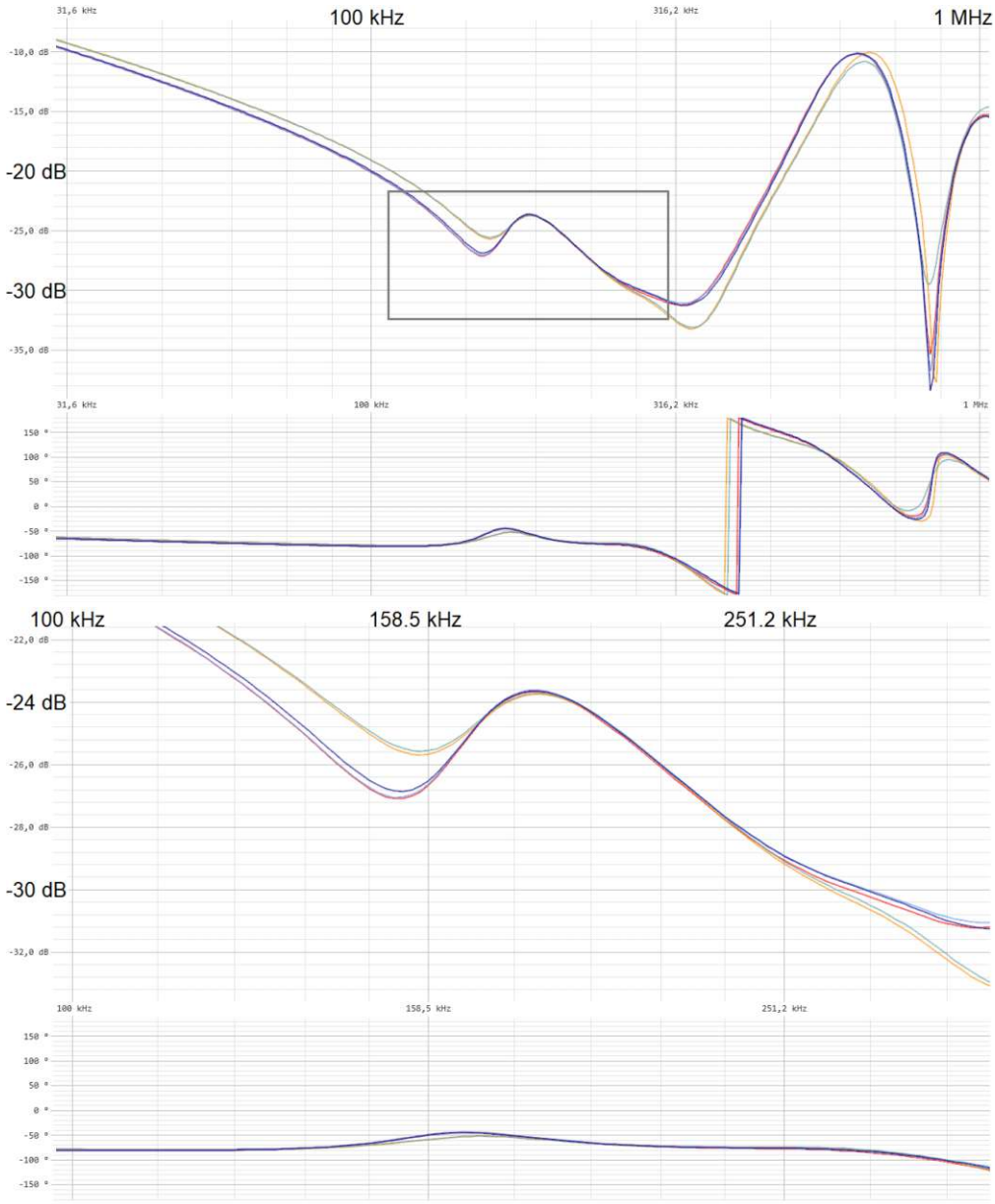

Figure 4.20: Inter-winding faults of *stator 2*: Phase U (red), G-J (symmetric winding fault, light blue), H-J (asymmetric by 1 turn, dark blue), F-J (asymmetric by 4 turns, blue-green) and E-F (single inter-turn fault, orange). The lower figure is a close-up of the rectangle in the upper figure. The symmetric fault is nearly identical with the fingerprint U, while the one turn asymmetric fault is slightly above it. The 4-turn fault is quite similar to the single inter-turn fault and therefore clearly identifiable.

The phase comparison in figure 4.21 shows similar results as the fingerprint comparison. The amplitude gap increases up to 150 kHz. The phase shift does not appear significant, anyway it is above 200 kHz.

The relative factors in table 4.10 do not indicate a fault. Since one fulfilled SFRA fault condition is enough for a reliably fault identification, the 4-turn asymmetric inter-winding fault can be determined in the phase comparison by the amplitude gap.

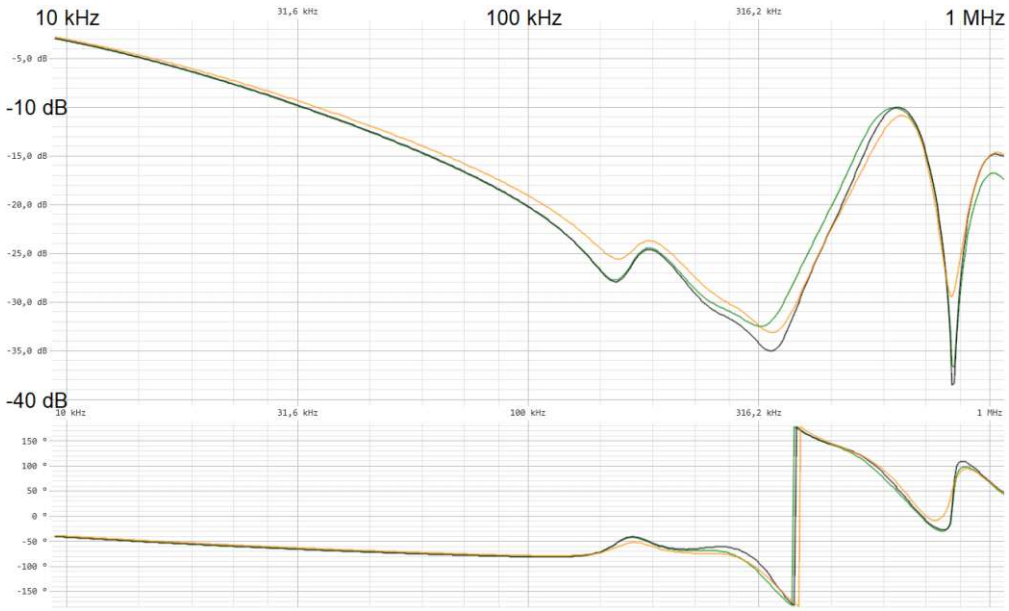

Figure 4.21: *Stator 2*: Phase comparison of an inter-winding fault: V (dark green), W (black) and F-J (asymmetric by 4 turns, orange).

Stator 1

Stator 1 (figure 4.22) shows even clearer results for inter-winding fault detection. All measured asymmetric faults are detectable by all three fault conditions. The similarity between the trends of the inter-winding and inter-turn faults also shows up in these measurements.

Stator 1		U	V	W
A-J	0t	4.18	3.90	2.21
C-J	3t	1.28	1.26	1.23

Table 4.11: Relative factors R_{LF} of *stator 1*. For the calculation, figure 4.22 is compared to the measurement before the access point installation. As the values show, the asymmetric fault is also detectable by the last fault condition (R_{LF} <2).

Figure 4.22: *Stator 1*: The symmetric fault A-J (orange) is nearly undistinguishable from the fingerprint U (red). Inter-winding fault C-J (asymmetric by 3 turns, light blue) is very close to the inter-turn fault A-B (2 turns, dark blue). The asymmetric fault is explicitly diagnosable by the fingerprint as well as by phase comparison since the amplitude gap and resonance shift condition are fulfilled.

Stator 3

Stator 3 represent similar results in figure 4.23. All asymmetric faults fulfill the amplitude gap and the phase shift fault condition and are, thus, reliably identifiable. The inter-turn fault A-E (15 turns) is nearly indistinguishable from the inter-winding fault E-K (asymmetric by 15 turns). Furthermore, all asymmetric faults show relative factor below 2 and are determinable by this fault condition as well (table 4.12).

Stator 3	U	V	W
A-K	0t	4.88	3.02	2.47
C-K	7t	1.41	1.56	1.21
E-K	15t	1.39	1.53	1.19

Table 4.12: Relative factors R_{LF} of *stator 3*. For the calculation, figure 4.23 is compared to the measurement before the access point installation. For the asymmetric faults, the condition R_{LF} <2 is fulfilled and therefore the faults are identifiable.

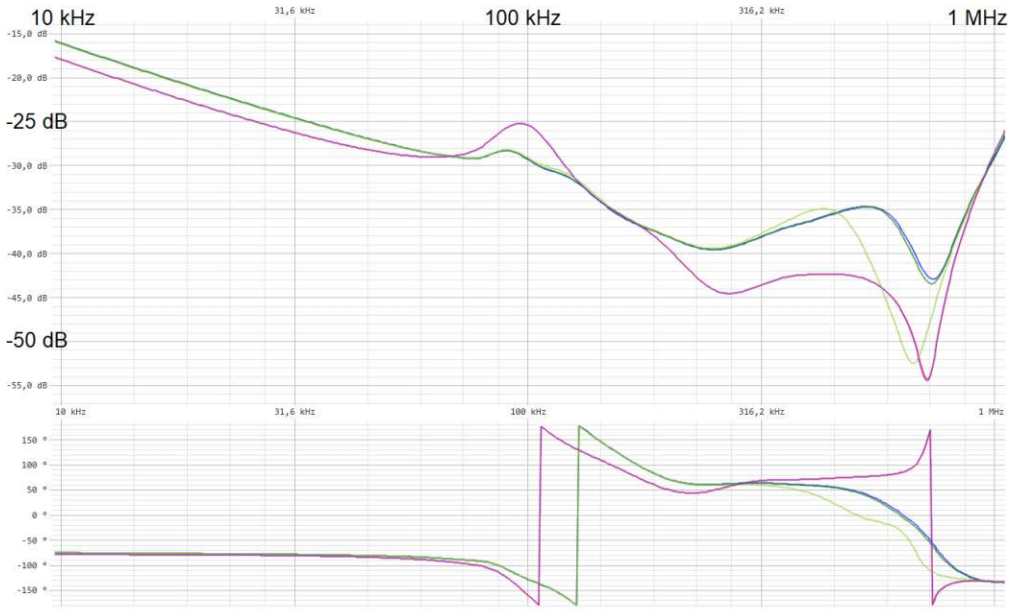

Figure 4.23: *Stator 3*: The symmetric case A-K (purple) is identical to the fingerprint *U* (red). It is interesting that E-K (asymmetric by 15 turns, dark green) is nearly undistinguishable from the inter-turn fault A-E (15 turns, blue). Fault C-K (asymmetric by 7 turns) is also similar to A-E over a wide frequency range. All asymmetric faults fulfill the amplitude gap and resonance shift fault condition, therefore, the malfunction can be identified.

Comparison with IFRA

The IFRA measurement in figure 4.24 shows the tested inter-winding faults of *stator 2*. The symmetric and 1-turn asymmetric fault are not detectable, neither with the fingerprint (table 4.13) nor the phase comparison (table 4.14). Only the 4-turn asymmetric fault fulfills the condition and differs by more than 10% in both comparisons (fingerprint and phase comparison).

Fingerprint compared to:	G-J (0t)	H-J (1t)	F-J (4t)
Area size comparison	0.2%	2.0%	15.0%
Differential area comparison	1.9%	6.5%	41.9%

Table 4.13: *Stator 2*: fingerprint measurement of inter-winding faults.

Phase V compared to:	G-J (0t)	H-J (1t)	F-J (4t)
Area size comparison	1.2%	2.9%	15.7%
Differential area comparison	8.2%	12.8%	46.7%
Phase W compared to:	G-J (0t)	H-J (1t)	F-J (4t)
Area size comparison	1.1%	2.8%	15.8%
Differential area comparison	2.5%	7.2%	42.6%

Table 4.14: *Stator 2*: Phase comparison of inter-winding faults.

The values of *stator 1* (table 4.15) and *stator 3* (table 4.16) represent an inter-winding fault sensitivity close to the SFRA measurement. It is possible to identify larger faults, but minor malfunctions stay unidentifiable.

IFRA of *Stator 1*	A-J (0t)	C-J (3t)
Area size comparison	0.6%	14.2%
Differential area comparison	1.4%	42.2%

Table 4.15: *Stator 1:* Fault to fingerprint comparison of inter-winding faults.

IFRA of *Stator 3*	A-K (0t)	A-J (28t)
Area size comparison	0.1%	26.4%
Differential area comparison	0.8%	98.7%

Table 4.16: *Stator 3:* Fingerprint measurement of inter-winding faults.

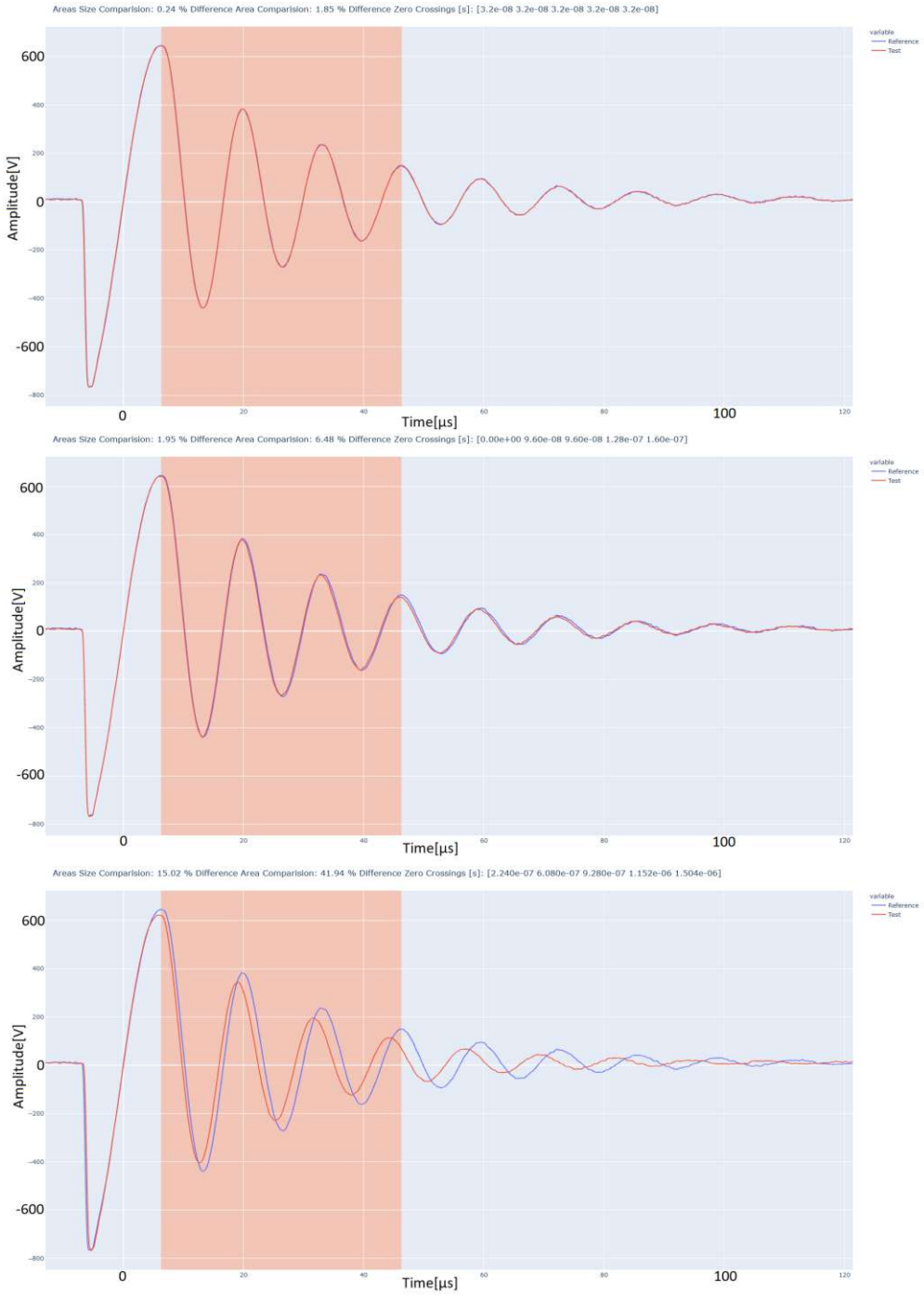

Figure 4.24: *Stator 2*, the healthy phase U (fingerprint) is always the reference (blue). The upper figure shows the comparison to the symmetric inter-winding fault G-J, the middle figure the 1-turn asymmetric fault H-J and the lower figure the 4-turn asymmetric fault F-J.

4.4 Reliability

All previous tests have been realized with full short circuits. For the reliability evaluation, a single turn is short-circuited with different resistances. The fingerprint comparison (figure 4.25) illustrates the executed test with 0.1 Ω, 1 Ω and 3.3 Ω. The first two faults fulfill the resonance shift condition, observable in the phase plot, and 0.1 Ω furthermore the amplitude gap condition. Hence, they are both identifiable. The 3.3 Ω fault is too close to the fingerprint to guarantee the recognizability under more difficult testing conditions.

The relative factors in table 4.17 show that $R_{LF}<2$ is only given for 0.1 Ω.

The phase comparison (figure 4.26) reveals only 1 Ω or lower short-circuited turns as faults. The deviation of the plot is recognizable, on the one hand, by the shift in the phase visualization, on the other hand, by the discernible lower amplitude of the resonance spot (first peak at 70 kHz).

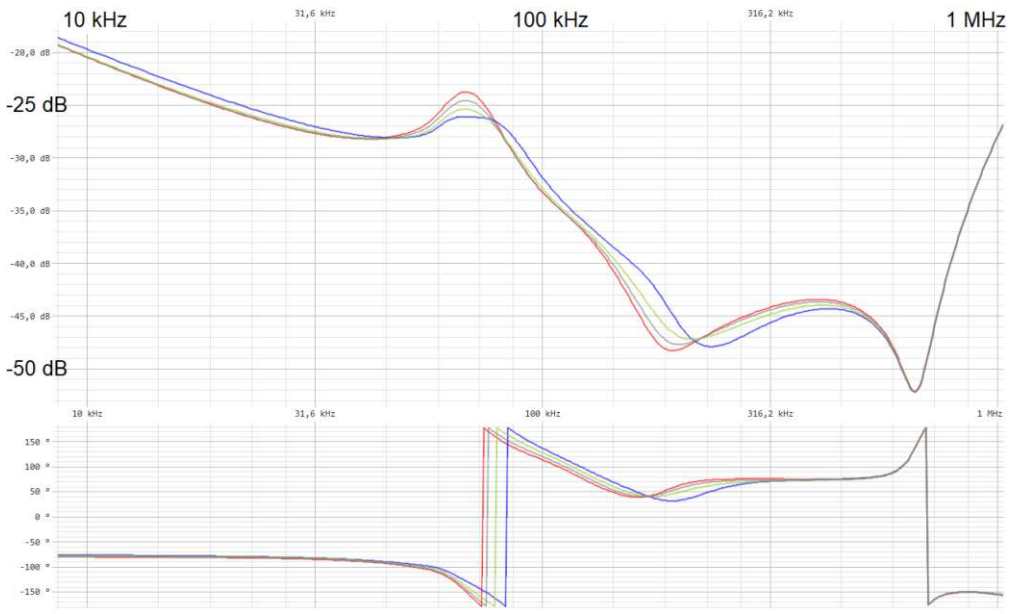

Figure 4.25: *Stator 1*, reliability evaluation, C-D short-circuited: fingerprint U (red), 0.1 Ω (blue), 1 Ω (light green) and 3.3 Ω (grey).

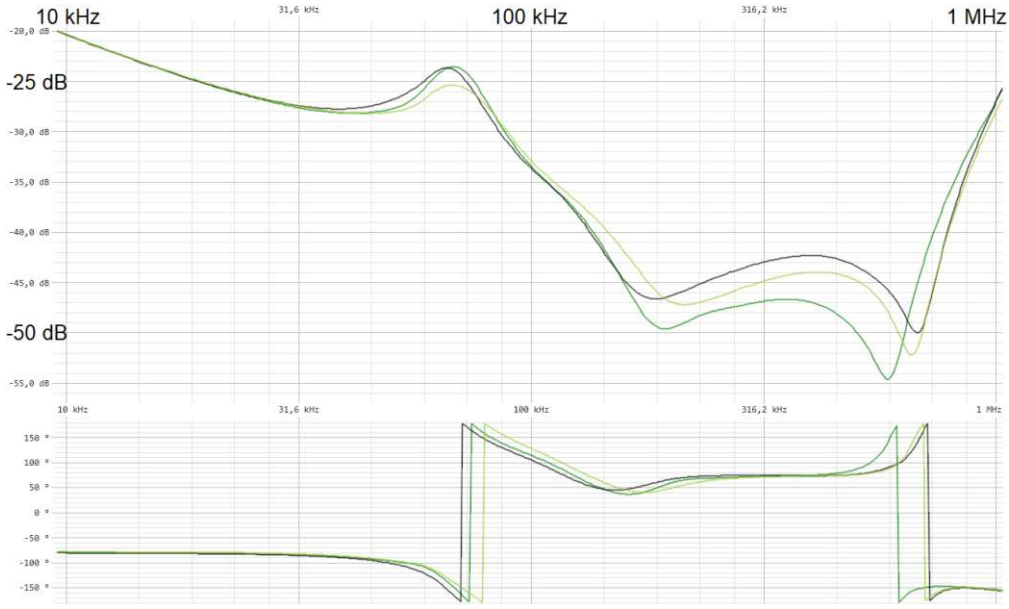

Figure 4.26: *Stator 1*, phase comparison, reliability evaluation: V (dark green), W (black) and 1 Ω (C-D, light green).

C-D short-circuited by	U	V	W
0.1 Ω	1.59	1.57	1.40
1 Ω	2.19	2.13	1.84
3.3 Ω	2.99	2.84	2.13

Table 4.17: *Stator 1*: Relative factors R_{LF} of the reliability evaluation. The values are generated from the plots in figure 4.25 and 4.26.

Comparison with IFRA

The impulse method has a similar reliability. Faults short-circuited by 1 Ω or lower fulfill the fault condition, short circuits with 3.3 Ω or higher miss them (table 4.18).

C-D short-circuited by	U		V		W	
0.1 Ω	17.1%	33.3%	19.0%	32.3%	18.2%	42.2%
1 Ω	13.3%	14.5%	15.5%	15.7%	14.6%	21.0%
3.3 Ω	5.4%	5.5%	7.5%	7.7%	6.5%	13.4%

Table 4.18: *Stator 1*: first column of a phase shows the area size difference, the second column the differential area comparison.

4.5 Winding Extension

More powerful induction motors (or generators) came along with bigger physical dimensions and, thus, larger and longer windings. In order to simulate a longer winding, the three phases of one stator are in series connection (figure 4.27). In this attempt, nodes of the parallel circuits are also located after one and two thirds of the winding, and not just at the beginning and at the end, which is usually the case in stators. Therefore, this setup is not fully representable and gives only an outlook of the possible behavior of longer windings. The three comparison phases differ in the sequence of U, V and W:

- Phase 1: **U**-V-W Implemented faults are at the beginning.
- Phase 2: V-W-**U** Implemented faults are at the end.
- Phase 3: W-**U**-V Implemented faults are in the middle.

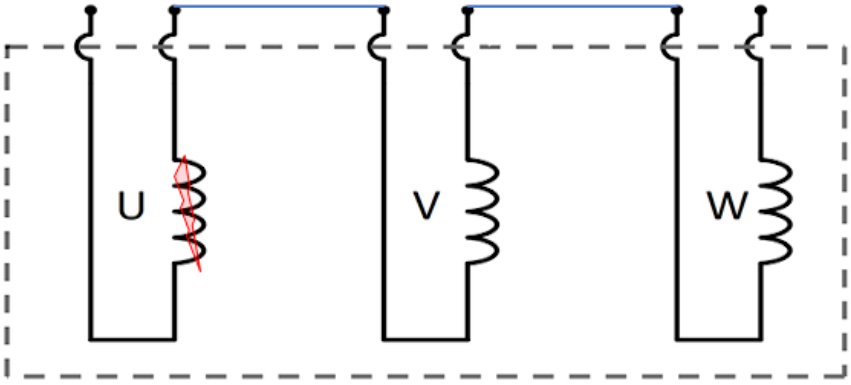

Figure 4.27: Setup for the extended winding attempt (phase 1).

Stator 1

Figure 4.28 shows the comparability of the phases, which reveals a minor deviation in the amplitude plot of phase 2 for *stator 1*. The discrepancy appears in the relative factor table (4.19) as well. Nevertheless, single inter-turn faults are reliably detectable in the fingerprint comparison as well as in the phase comparison.

The measurement of *stator 1* in figure 4.29 reveals an interesting behavior of the fault phase. It seems that the plots depend on the position of the short-circuited turn, which should have no influence according to section 4.1 (directionality). However, they still fulfill certain fault conditions: D-E in phase 1 shows a shift of the first resonance,

identifiable by the shift of the saltus and a displacement of the peak in the amplitude visualization. D-E in phase 2 does the same with an additional shift at the second saltus. D-E in phase 3, where the fault is in the middle of the winding, only differs from the healthy phases at the second saltus.

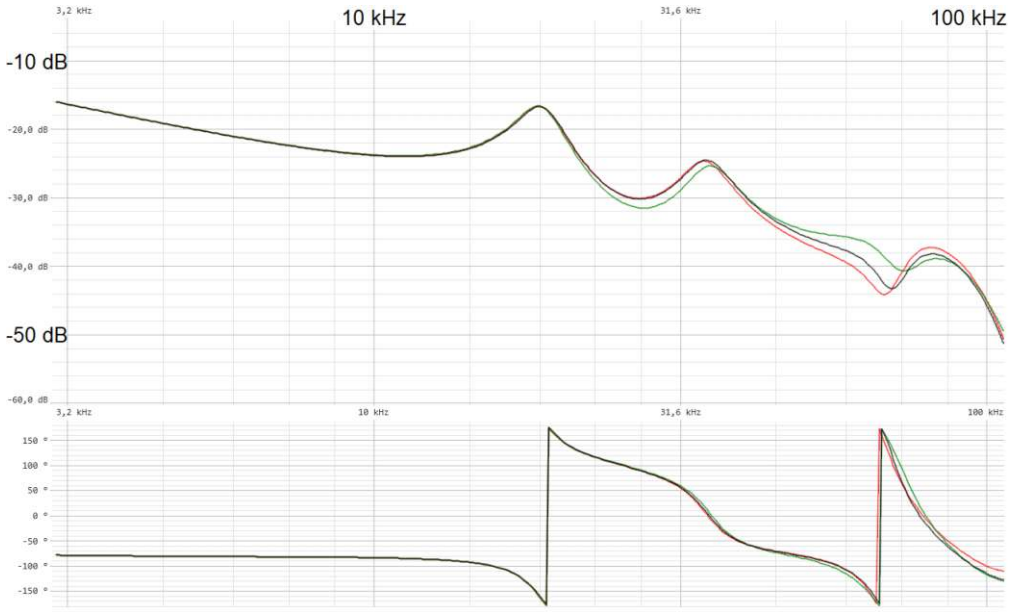

Figure 4.28: Phase comparison of *Stator 1*: phase 1(red), phase 2 (green) and phase 3 (black).

The relative factors of *stator 1* (table 4.19) identify all three cases as faults, hence a second fault condition is fulfilled. However, this table would also lead to the wrong assumption that phase 2 contains a malfunction.

	Phase 1	Phase 2	Phase 3
Phase 1	6.16	1.56	2.23
Phase 2	1.56	6.63	1.98
Phase 3	2.23	1.98	7.18
D-E in Phase 1	1.75	1.41	1.80
D-E in Phase 2	1.24	1.76	1.50
D-E in Phase 3	1.12	1.17	1.26

Table 4.19: Relative factors of the extended phases of *stator 1*: The plots in figure 4.29 are compared to a measurement executed 2 hours earlier.

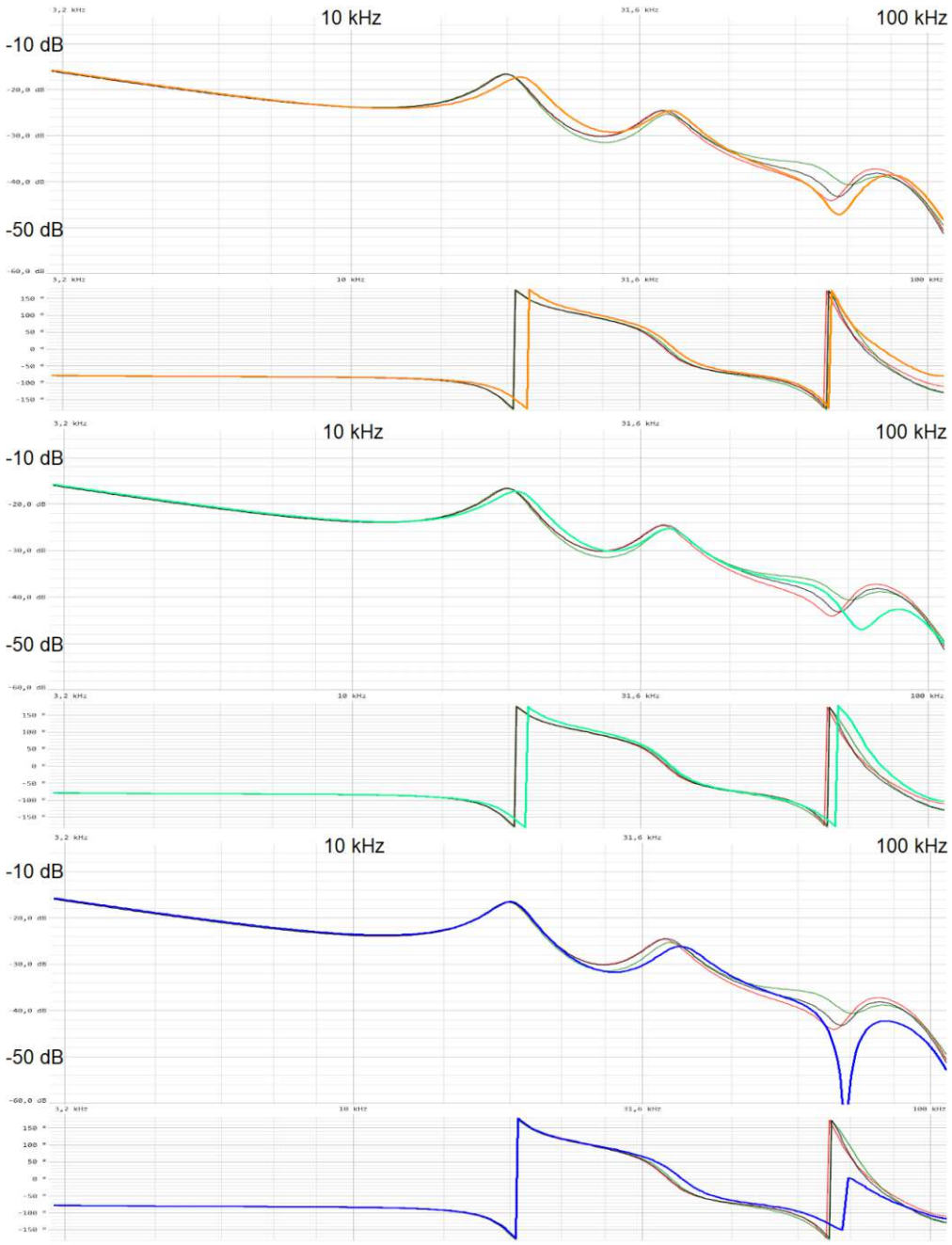

Figure 4.29: Extended winding measurement of *stator 1*: phase 1 (red), phase 2 (green) and phase 3 (black), compared to the single inter-turn fault D-E implemented in phase 1 (upper figure, fault at the beginning), phase 2 (middle figure, fault at the end) and phase 3 (lower figure, fault in the middle). For a better visualization, the figures are squeezed so that all images are one underneath the other on one side.

Stator 2

The measurements of *stator 2* (4.30) show similar results. The fault implemented in phase 1 or 2 generate resonance shifts, while the fault in the middle of the winding is detectable only from the amplitude deviation from the fingerprint.

The relative factors (table 4.20) identify all healthy phases and the faults at the beginning and at the end correctly. Merely E-F in the middle of the winding is too close to the phases to be determined as a fault.

For both stators, the fault in the middle is the most difficult to detect. This might be owing to the additional nodes after the first and second third of the extended winding. Nonetheless, the faults are identifiable by the defined fault conditions, although more research of longer stator windings is needed.

	Phase 1	Phase 2	Phase 3
Phase 1	6.91	3.01	3.67
Phase 2	3.01	7.10	2.84
Phase 3	3.67	2.84	8.02
E-F in Phase 1	1.48	1.45	1.46
E-F in Phase 2	1.45	1.42	1.42
E-F in Phase 3	2.41	2.43	2.37

Table 4.20: Relative factors of the extended phases of *Stator 2*: The plots in figure 4.30 are compared to a measurement executed 2 hours earlier.

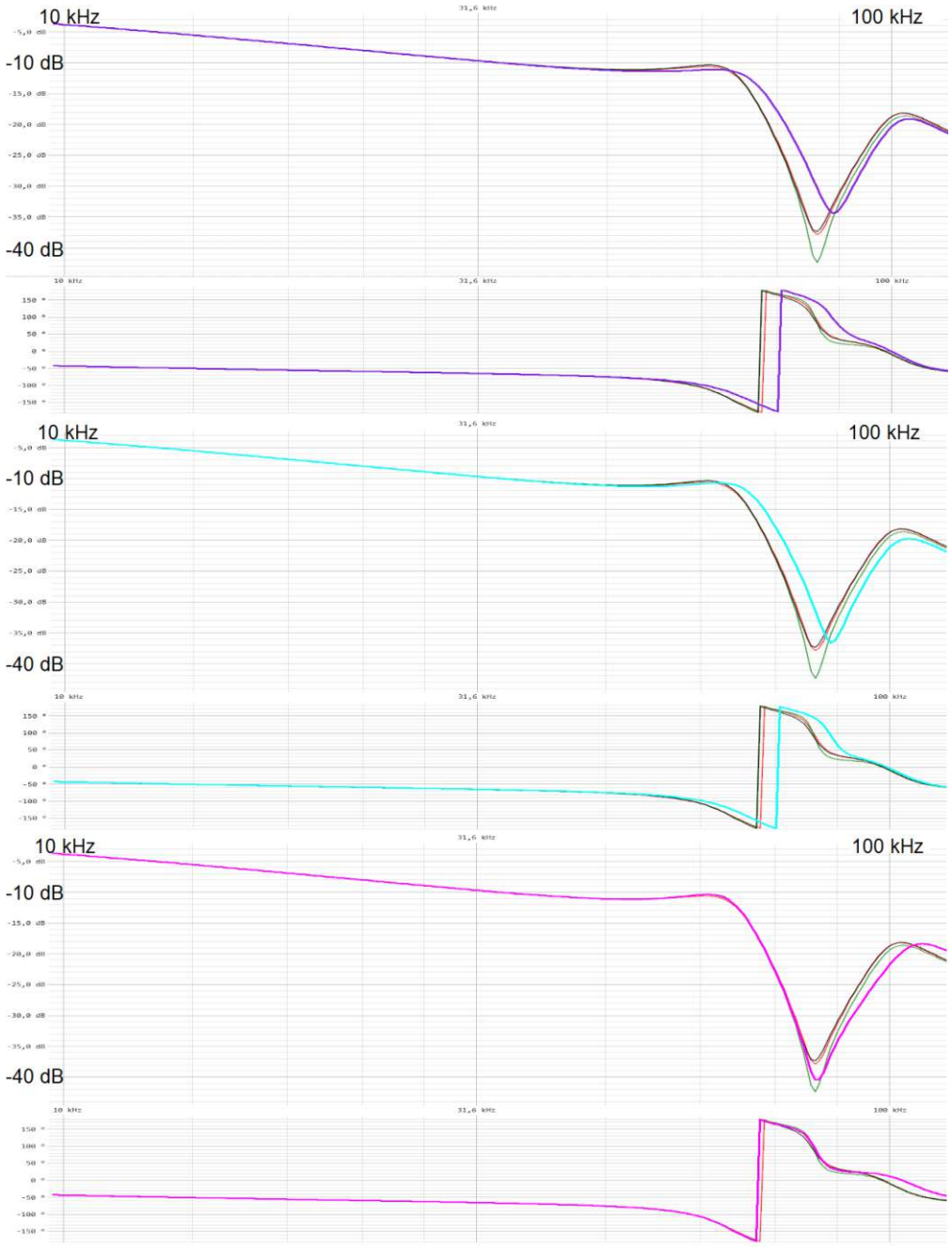

Figure 4.30: Extended winding measurement of *stator 2*: phase 1 (red), phase 2 (green) and phase 3 (black) compared to the single inter-turn fault E-F implemented in phase 1 (upper figure, fault at the beginning), phase 2 (middle figure, fault at the end) and phase 3 (lower figure, fault in the middle). The fourth color in each plot shows the fault case. For a better visualization, the figures are squeezed so that all images are underneath one another on one side.

Comparison with IFRA

The IFRA fingerprint comparisons of the extended winding are shown in figure 4.31. The size of the fault's impact increases with the distance to the input terminal, which corresponds to section 4.1 (directionality). Still, the values for the area size and differential area comparison (table 4.21) do not indicate a fulfilled fault condition for any measurement.

Stator 1	P1-P2	P1-P3	P2-P3
Area size comparison	1.5%	0.4%	2.0%
Differential area comparison	2.3%	8.2%	9.1%
Fault to fingerprint comparison			
D-E in	P1	P2	P3
Area size comparison	3.1%	2.6%	4.6%
Differential area comparison	14.1%	39.4%	15.5%

Table 4.21: IFRA quantifying values for the extended windings of *stator 1*: comparison of the healthy phases and fault-to-fingerprint comparison.

The values for *stator 2* (table 4.22 and figure 4.32) exhibit a similar result, which also does not enable a precise identification of short circuits in the winding with the defined conditions.

Stator 2	P1-P2	P1-P3	P2-P3
Area size comparison	0.8%	0.5%	1.3%
Differential area comparison	4.8%	3.4%	8.1%
Fault-to-fingerprint comparison			
E-F in	P1	P2	P3
Area size comparison	2.2%	1.6%	5.2%
Differential area comparison	4.6%	3.8%	16.5%

Table 4.22: IFRA quantifying values for the extended windings of *stator 2*: comparison of the healthy phases and fault-to-fingerprint comparison.

Overall, it is very difficult to detect a malfunction in a longer winding with the IFRA method. Another indication that the IFRA method is poorly suited for longer windings is the increasing deviation of the curve from the waveform of a damped oscillation, most distinctive at the first two to three peaks.

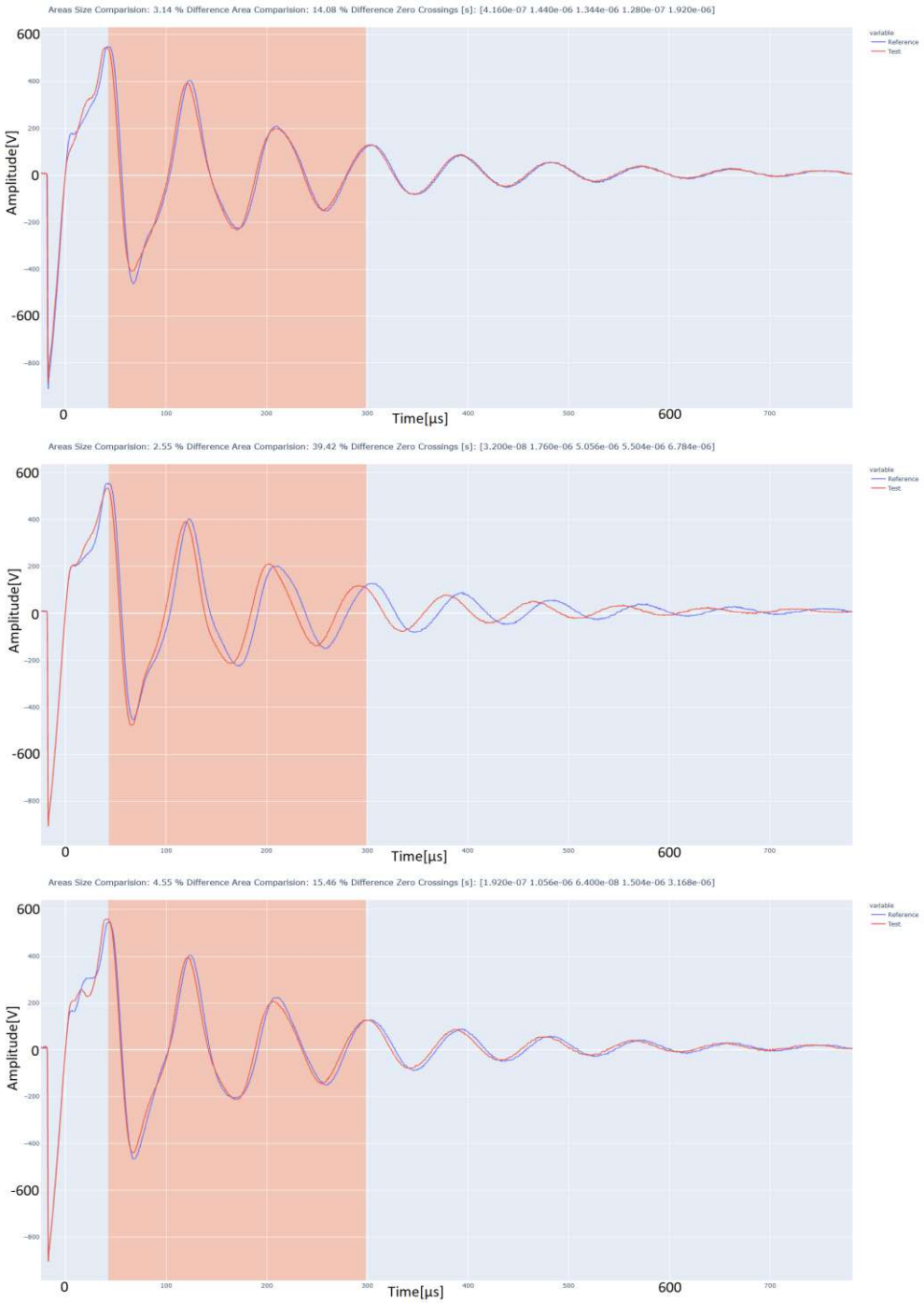

Figure 4.31: Extended winding measurement of *stator 1*: fault-to-fingerprint comparison of phase 1 (upper figure, fault at the beginning), phase 2 (middle figure, fault at the end) and phase 3 (lower figure, fault in the middle). In each case, the healthy fingerprint of a phase (reference) is blue and the same phase containing a one-turn fault is red.

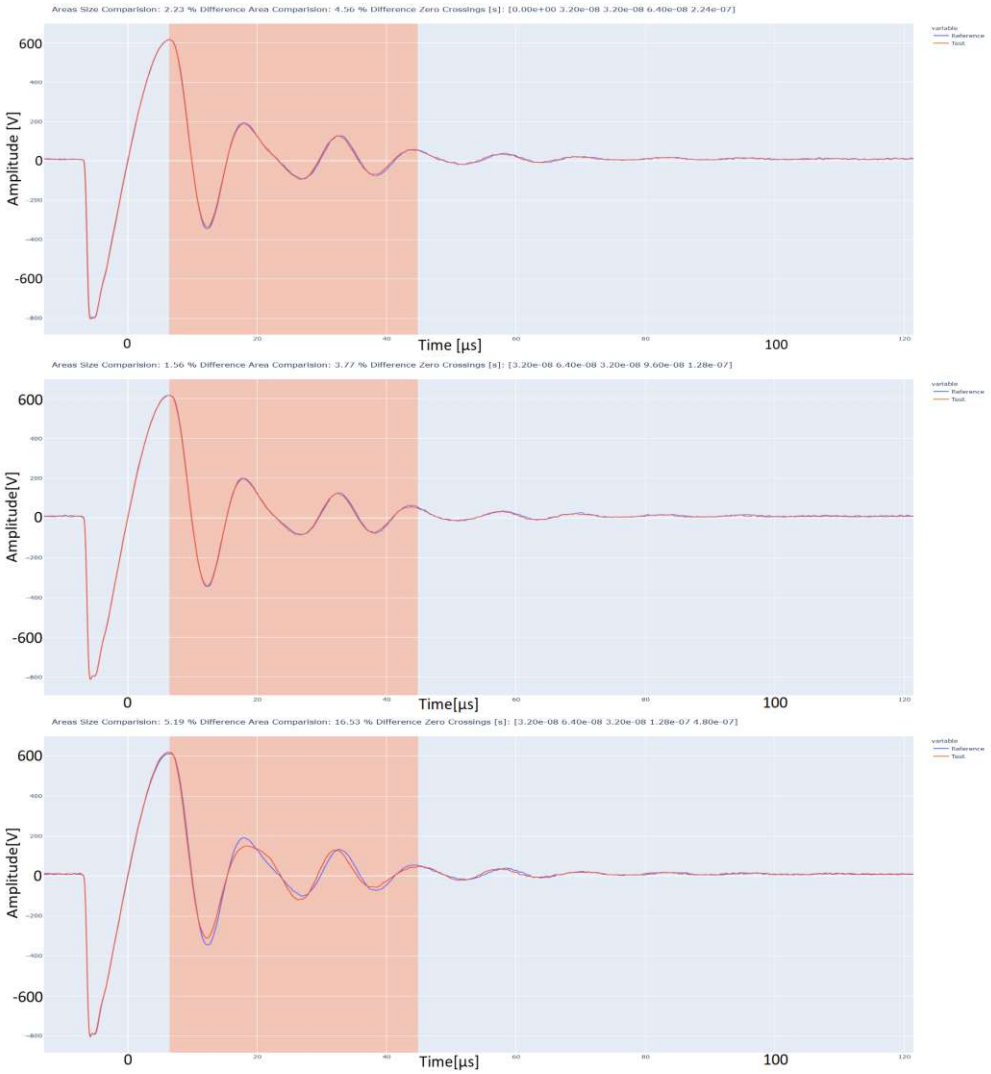

Figure 4.32: Extended winding measurement of *stator 2*: fingerprint comparison of phase 1(upper figure, fault aut the beginning), phase 2 (middle figure, fault at the end) and phase 3 (lower figure, fault in the middle). In each case, the healthy fingerprint of a phase is blue and the same phase containing a one-turn fault is red.

5 Conclusion

The brand-new stators guaranteed an absolute healthy and flawless condition at the beginning of the measurements. The comparison of the tests before and after soldering the access points to the winding proves that there is only a negligible impact caused by the manipulation installation.

The defined fault conditions for the SFRA method proved their value, but could still be developed further. For example, the amplitude gap could be quantified with a differential area calculation. The resonance shift criterion underlines the importance of the phase plot and could be enhanced with a defined threshold value. The relative factors of the low frequency range also verified themselves as reliable fault indicators. The R_{FL}<2 threshold from the power transformer seems to fit for stators as well. If at least one of these conditions is fulfilled below 200 kHz, this is trustworthy evidence for a malfunction of the tested machine. The frequency range above 200 kHz is increasingly influenced by the equipment and more research is required to gain further information about the winding's health from this frequency range.

The IFRA phase comparisons of *stator 1* and *3* (table 4.9 and 4.8) demonstrate the necessity that both quantifying values, area size and difference area comparison, have to be larger than 10% for a clear identification of a short circuit.

The deviation between the phases (measured with SFRA as well as IFRA) could be explained by the fact that each phase comprises a different angle of the winding head, which leads to different capacities.

The results show multiple advantages of the SFRA method compared to the surge test, starting with the independence of the measurement direction and thus the position of the fault. Identical short circuits always exhibit the same effect on the curve. Furthermore, the same winding structure (*stator 1* and *3*) generates similar plots (figure 4.10), which could be very interesting in the future for virtually generated references.

Inter-turn faults usually trigger all three fault SFRA conditions, and at least one is always fulfilled. Actually, single short-circuited turns are clearly detectable even in the

phase comparison. This implies the possibility of identifying a winding loss smaller than 1% (i.e. short-circuited turns divided by the number of turns of one parallel circuit).

Inter-winding faults are also determinable by SFRA, as long as they are not symmetric or close to symmetric faults. Faults with 3 or more turns asymmetry fulfill at least one condition and are thus unambiguous. These faults show a nearly identical effect on the curve as the inter-turn faults. The surge test of inter-winding faults presents similar results.

The reliability measurement reveals nearly the same result for both methods used. Single inter-turn faults with up to 1 Ω resistance are possible to detect, 3.3 Ω or above do not trigger the fault conditions.

The attempt with the extended windings is only partly representative for bigger stators but still provides an interesting outlook for the method's applicability on longer windings. The SFRA measurement is definitely more suited for this task than the impulse method and was able to determine all three fault cases, although some advantages, such as the independence of the fault position, are no longer given. This might be caused by the additional nodes after one and two thirds of the winding. The IFRA method was not capable to detect one single fault with the defined criterions.

Strictly speaking, all findings are scientifically proven only for the three tested stators.

Last but not least, SFRA ensures greater safety since the operating voltages are at a low level.

Sweep frequency response analysis has the potential to be one of the future standard diagnostic tests for rotating machines. This noninvasive method is well suited for this task, and the possibility of the phase comparison enables the applicability in already operating machines. One day the measurements might also be assisted by computer-generated curves, which would further improve the diagnostic possibilities. Until then, more research has to be done to verify the results for larger machines (in the MW range) and to define threshold values for the separate fault conditions.

Bibliography

[1] Association, IEEE S. u. a.: IEEE Guide for the Application and Interpretation of Frequency Response Analysis for Oil-Immersed Transformers, IEEE Std C57. 149 2012. In: *IEEE Power and Energy Society* 8 (2013)

[2] Blánquez, FR ; Platero, CA ; Rebollo, E ; Blázquez, F: Field-winding fault detection in synchronous machines with static excitation through frequency response analysis. In: *International Journal of Electrical Power & Energy Systems* 73 (2015), S. 229–239

[3] China, The Electric Power Industry S. o.: *Frequency Response Analysis on Winding Deformation of Power Transformers*. 2005. – Promulgated by National Development and Reform Commission of Republic of China

[4] Ciancetta, Fabrizio ; Pizzo, Andrea del ; Olivieri, Carlo ; Rotondale, Nicola ; Castellini, Luca ; d'Andrea, Moreno: SFRA technique applied to fault diagnosis on stators of electric motors. In: *2014 International Symposium on Power Electronics, Electrical Drives, Automation and Motion* IEEE, 2014, S. 515–520

[5] Dorf, Richard C.: *Circuits, signals, and speech and image processing*. CRC Press, 2006

[6] IEC, 60034-18-32: Rotating Electrical Machines - Part 18-32: Functional evaluation of insulation systems. (2010)

[7] Khalilisenobari, Reza ; Sadeh, Javad: Electrical Machines Fault Detection through Frequency Response Analysis (FRA)–Part I: Stator. In: *arXiv preprint arXiv:2002.06695* (2020)

[8] Kolerus, Josef ; Wassermann, Johann: *Zustandsueberwachung von Maschinen*. expert verlag, 2008

[9] Mugarra, Asier ; Platero, Carlos A. ; Martínez, Jose A. ; Albizuri-Txurruka, Unai: Validity of Frequency Response Analysis (FRA) for Diagnosing

Large Salient Poles of Synchronouos Machines. In: *IEEE Transactions on Industry Applications* 56 (2019), Nr. 1, S. 226–234

[10] OMICRON: *Brochure and Datasheet FRANEO 800*

[11] OMICRON: *FRANEO 800*. https://www.omicronenergy.com/de/produkte/franeo-800/, . – Stand: 24.9.2020

[12] OMICRON: *Operation Manual CPC 100*

[13] OMICRON: *Operation Manual FRANEO 800*

[14] RÄDLER, Michael ; UHRIG, Stephanie: Performing reliable and reproducible frequency response measurements on power transformers. In: *Transformers Magazine* 5 (2018), Nr. 3, S. 42–49

[15] Raedler, Michael ; Uhrig, Stephanie ; Velasquez Contreras, Juan L.: Electrical interferences in SFRA measurements. In: *Transformers Magazine* 4 (2017), Nr. 2, S. 60–70

[16] SKF: The State of Surge Testing On Induction Motors, 2013

[17] Sourcetronic, GmbH: *Operation Manual MODEL ST2883-5/-10*

[18] Standard, IEC: 60076-18. In: *Measurement of frequency response, Edition* 1 (2018), Nr. 0, S. 2012–07

[19] Tektronix: *Benutzerhandbuch Serien DPO2000 und MSO2000 Oszilloskope*

[20] Tonghui, Electronics: *Operation Manual Impulse Winding Tester MODEL TH2883-5/-10*

[21] Uhrig, Stephanie ; Oettl, Fabian ; Augeneder, Norbert ; Hinterholzer, Reinhard: Diagnosemoeglichkeiten an rotierenden Maschinen mittels FRA und zu beachtende Einfluesse. In: *VDE-Hochspannungstechnik* (2018)

[22] Wilson, John: Current state of surge testing induction machines. In: *Iris Rotating Machine Conference*, 2003, S. 1–13

Acknowledgement

First of all, I would like to thank Martin Gröschl and Fabian Öttl for the opportunity to realize this thesis and to give something back to the scientific world. Whenever I needed help or had questions they took their time to explain me even the obvious things. I had a lot of fun doing "Jugend forscht" and enjoyed the freedom of trying out whatever came to my mind.

But it was a long journey until the end of this thesis, way longer than 66 sheets of paper, during which wonderful people surrounded me.

I would like to thank my girlfriend Sarah for her support, her encouragement and her enthusiasm (sometimes even for physics).

Many thanks to my university buddies Jan, Magda, Lisa and Basti, as well as to the best flatmate Flo, the best upstairs neighbor Jessi, and my personal allrounder Lukas.

Last but not least, thanks to my mum, my dad and my brothers Theo, Paul and Fridolin, as well as my cousins Miriam and Manuel - you always had my back.